1.0

4.5
5.0
5.6

2.8

2.5

3.2

2.2

3.6

1.1

4.0

2.0

1.8

1.25

1.4

1.6

MICROCOPY RESOLUTION TEST CHART

NATIONAL BUREAU OF STANDARDS-1963-A

AFGL-TR-85-0076

DETAILED SPHERICAL-HARMONIC REPRESENTATION
OF THE EARTH'S GRAVITY FIELD AND TIDAL EFFECTS
FROM ALTIMETRIC ADJUSTMENTS

Georges Blaha

Nova University Oceanographic Center
8000 North Ocean Drive
Dania, Florida 33004

Final Report
Period covered 1 January 1982 - 31 December 1984

February 1985

Approved for public release; distribution unlimited
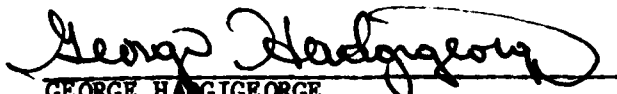
CONTRACTOR REPORTS

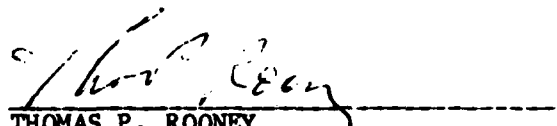This technical report has been reviewed and is approved for publication.

GEORGE HADGIGEORGE
Contract Manager

THOMAS P. ROONEY
Chief, Geodesy & Gravity Branch

FOR THE COMMANDER

DONALD H. ECKHARDT
Director
Earth Sciences Division

REPORT DOCUMENTATION PAGE		READ INSTRUCTIONS BEFORE COMPLETING FORM
1. REPORT NUMBER AFGL-TR-85-0076	2. GOVT ACCESSION NO. AD-A160419	3. RECIPIENT'S CATALOG NUMBER
4. TITLE (and Subtitle) DETAILED SPHERICAL-HARMONIC REPRESENTATION OF THE EARTH'S GRAVITY FIELD AND TIDAL EFFECTS FROM ALTIMETRIC ADJUSTMENTS		5. TYPE OF REPORT & PERIOD COVERED Final Report Period covered 1/1/82-12/31/84
		6. PERFORMING ORG. REPORT NUMBER
7. AUTHOR(s) Georges Blaha		8. CONTRACT OR GRANT NUMBER(s) F19628-82-K-0007
9. PERFORMING ORGANIZATION NAME AND ADDRESS Nova University Oceanographic Center 8000 North Ocean Drive Dania, Florida 33004		10. PROGRAM ELEMENT, PROJECT, TASK AREA & WORK UNIT NUMBERS 61102F 2309G1BB
11. CONTROLLING OFFICE NAME AND ADDRESS Air Force Geophysics Laboratory Hanscom AFB, Massachusetts 01731 Contract Monitor: George Hadgigeorge/LWG		12. REPORT DATE February 1985
		13. NUMBER OF PAGES 94
14. MONITORING AGENCY NAME & ADDRESS(if different from Controlling Office)		15. SECURITY CLASS. (of this report) Unclassified
		15a. DECLASSIFICATION/DOWNGRADING SCHEDULE

16. DISTRIBUTION STATEMENT (of this Report)

Approved for public release; distribution unlimited.

17. DISTRIBUTION STATEMENT (of the abstract entered in Block 20, if different from Report)

18. SUPPLEMENTARY NOTES

19. KEY WORDS (Continue on reverse side if necessary and identify by block number)

Satellite altimetry	Spherical harmonics	Equilateral grid
Short-arc adjustment	Point masses	Smoothing effect
Geoid undulations	Collocation with noise	Tidal constituents
Gravity anomalies	Residuals	Ocean tide

20. ABSTRACT (Continue on reverse side if necessary and identify by block number)

Two second-phase techniques have been developed in recent years at AFGL based on the results of the global spherical-harmonic treatment of altimetric data. One of these techniques has been documented as the point-mass adjustment, and the other has been described under the name of modified collocation with noise. The term "modified" does not concern the philosophy of the least-squares collocation with noise, but, rather, its specific application aimed at describing a smoothed-out gravity field, in which the part of the signal beyond the desired smoothing —

DD FORM 1473   EDITION OF 1 NOV 65 IS OBSOLETE
1 JAN 73

level is pushed into the realm of "noise".

The primary task ~~addressed in this report~~ consists in representing collocation results in terms of the spherical-harmonic expansion of the geopotential. In particular, an equilateral grid of geoid undulations (referring to a higher order surface than an ellipsoid) predicted through the modified collocation with noise at the smoothing level (n',n') can be utilized in a numerical integration algorithm, eventually producing an (n',n') set of spherical-harmonic coefficients consistent with the collocation results. The conditions under which the consistency requirement is satisfied are analyzed in computer simulations.

As the most important outcome of these simulations, the familiar rule of thumb is singled out as an accurate and clearcut indicator of the highest degree and order spherical-harmonic model (N,N) which can still faithfully represent the gravity field as described by a discrete set of data -- here an equilateral grid of geoid undulations. This rule stipulates that $N=180°/\theta°$, where $\theta°$ symbolizes the grid interval in angular measure. It is observed that up to the degree n'=N, the r.m.s. of the errors in geoid undulations imputable to the numerical integration is comfortably small and increases at a very low rate for increasing n', while beyond the degree N the situation worsens drastically. Similar results are produced when errors in gravity anomalies are considered.

Several other topics are addressed in this report as well, such as the comparison between the single- and the double-layer point-mass adjustment, the detailed gravity field resolution in areas of special interest via third-phase adjustments, the possibility of introducing tidal point masses into the existing point-mass adjustment, the utilization of altimeter residuals for a detection of bathymetric and other oceanic anomalies, and the global representation of tidal effects with the aid of spherical-harmonic tidal coefficients. The last subject is especially important, in that it leads to the inclusion of new and accurate information into the adjustment of specific tidal parameters (the tidal amplitude and the Greenwich phase angle per constituent) within the overall adjustment of satellite altimetry.

TABLE OF CONTENTS

TABLE OF CONTENTS (Continued)

LIST OF FIGURES

LIST OF TABLES

v

1. INTRODUCTION

The initial, or first-phase treatment of satellite altimeter data has been carried out at AFGL in a global short-arc adjustment of spherical-harmonic (S.H.) potential coefficients, state vector parameters and, optionally, certain tidal parameters. This least-squares adjustment is aimed at a long-wavelength resolution of the earth's gravity field and its fundamental surface, the geoid. It has been the subject of various AFGL reports and papers, e.g., [Blaha, 1981, 1982], and has been applied especially to SEASAT altimetry.

For the reasons recapitulated in [Blaha, 1981], the orbital arcs entering the adjustment have been limited to 7 minutes in duration, i.e., to 25.0° in angular length. Most of the satellite passes have been subdivided at the pre-processing level to satisfy this requirement, except for natural disruptions in the flow of data (gaps due to land masses, malfunction or the altimeter, etc.). Arcs shorter than 3° have been eliminated altogether. Because of the (14,14) degree and order truncation adopted in the S.H. adjustment model, the shortest half-wavelength of the geoidal resolution amounts to approximately 12.9° (this is $180^{\circ}/n$, with n=14, as given by the familiar rule of thumb). Accordingly, the arc length of 25° corresponds to the full wavelength of the smallest geoidal features to be represented by the adjustment.

In order to allow the fine structure of the earth's gravity field to be added to its long-wavelength features representing a new "reference field", second-phase techniques have been conceived based on the results from the first phase. One such technique has been designed in terms of the point-mass (P.M.) parameters, as described in several AFGL reports, e.g., [Blaha, 1983, 1984]. Due to the banded structure of the matrix of normal equations, the P.M. parameters can be resolved in overlapping strips, which can be combined together so as to cover the

whole oceanic geoid. Optionally, certain tidal parameters can also be included in such a least-squares adjustment; in this case the matrix of normal equations becomes banded-bordered, having the tidal parameters in the border.

The P.M. approach has recently been complemented by a specific modification of the least-squares collocation with noise, which provides another means for a second-phase gravity field resolution on a local, regional, or global scale. The modification resides in pushing a part of the signal, corresponding to the gravity field variations beyond the desired smoothing level, into the realm of "noise". A detailed description of this technique is offered in [Blaha, 1984].

Both second-phase approaches above are built on the altimeter residuals (taken as minus the geoidal residuals) from the first phase, utilized in the role of new observations. Thus, the high-resolution altimeter information enters the second phase, while the state vector parameters, the adjustment of which is the most time-consuming element in the treatment of altimeter data, are no longer considered at this stage.

The above two approaches are the topic of Chapter 2, which recapitulates their basic features and describes their ability to address particular tasks. One such task is concerned with designing a third-phase approach in view of a detailed gravity field representation in areas of special interest. Chapter 3 deals with the P.M. approach alone, in considering a double-layer version with its advantages and disadvantages.

In addition to describing the earth's gravity field, the outcome of the collocation approach can also serve in generating a set of S.H. potential coefficients which, under certain conditions, will accomplish the same task equally well. The process of representing collocation results by a S.H. expansion is outlined in Chapter 4, while the conditions under which such a representation is consistent

with the collocation outcome are analyzed in Chapter 5. This analysis is carried out primarily through computer simulations, in which extensive use is made of Legendre polynomials and associated Legendre functions. An accurate and efficient evaluation of the latter is the subject of Appendix 1.

The outcome of Chapter 5 is subsequently exploited in Chapter 6. Section 6.1 completes the development of Chapter 4, and thus rounds off the algorithm leading from the collocation results to a detailed S.H. representation of the earth's gravity field. And Section 6.2 uses some of the principles set forth in Chapter 5 in developing an algorithm for a global representation of tidal effects with the aid of S.H. tidal coefficients. Chapters 4-6 together with Appendix 1 could be combined in one larger unit representing the main thrust of the present study.

Subjects having a weaker link to the principal topics contained in the body of this report are relegated to Appendices 2 and 3. They deal, respectively, with the possibility of introducing tidal point masses into the P.M. adjustment, and with the utilization of altimeter residuals for a detection of bathymetric, geomagnetic, and other anomalies in open oceans. All three appendices, as well as most of the chapters, are presented essentially in a self-contained manner, and can thus be read independently without impairment to a good understanding of the presented material.

In addition to ,is Final Report, the reports dealing with satellite altimetry during the period of the present research contract have been [Blaha, 1983, 1984].

2. EVALUATION OF A LARGE-SCALE SECOND-PHASE GRAVITY FIELD REPRESENTATION AND A DETAILED RESOLUTION IN AREAS OF SPECIAL INTEREST

2.1 Point-Mass Approach

The point-mass (P.M.) adjustment is built on the adjusted geoid from the first phase which can represent a "normal field". The parameters in this method are the P.M. magnitudes associated with point masses distributed in an equilateral grid. The point masses can form a single layer, in which case they are all at the same depth below the surface of the reference ellipsoid, or a double layer, in which case there are twin point masses at each location of the grid, separated by a predetermined vertical distance. The number of parameters is the same in both these modes since a twin point mass represents only one parameter; the magnitudes of the shallower and deeper point masses are equal, only their signs differ. The resolution power depends primarily on the grid interval, and to a much lesser degree on their depth and/or vertical separation of the twin point masses. This is illustrated in Table 1 of the next chapter. Thus, for example, if the point masses (single or twin) are distributed in a $2^{\circ} \times 2^{\circ}$ equilateral grid, the resolution corresponds approximately to a (90,90) spherical-harmonic expansion.

The second-phase P.M. adjustment treats the new observations (minus the geoidal residuals from the first phase), the P.M. parameters and, optionally, certain tidal parameters in a simultaneous least-squares process leading to a more detailed resolution of the earth's gravity field on the global oceanic scale. In view of the banded or the banded-bordered structure of normal equations, an approximation is introduced through a cut-off distance beyond which the con-tribution of observations to a given P.M. parameter is ignored. Although only information representing the geoid undulations enters the adjustment in the

-4-

form of observed quantities, the solved for P.M. magnitudes allow the evaluation of other functions of the disturbing potential (with respect to the adopted "normal field") as well, given the geodetic coordinates on the earth's surface. It should be noted that due to the relatively high degree and order of the adopted reference field, such as the (14,14) spherical-harmonic (S.H.) field resolved during the first phase as compared to the ellipsoidal field, the spherical approximation introduced in the P.M. model is inconsequential.

The final outcome of the two adjustment phases with respect to the geoid and the earth's gravity field consists of a set of S.H. potential coefficients and the magnitudes of the point masses introduced at the predetermined locations, which enable one to determine geoid undulations, gravity anomalies, etc., at any points of interest (the latter usually form a geographic grid to be used for the construction of contour maps). Each such quantity is an algebraic sum of two parts, the first due to the S.H. coefficients and the second due to the P.M. parameters. The numerical values of such quantities, for example the values of geoid undulations covering the globe in a sufficiently dense grid, are considered to describe the earth's gravity field to within the desired resolution characterized by an equivalent S.H. expansion (n',n').

If the desired resolution should be very detailed, practical difficulties will manifest themselves when the second-phase adjustment encompasses the whole globe or a large ocean basin. Since the P.M. grid is increasingly dense in such cases, the resolution of a great many P.M. parameters becomes impossible from the standpoints of computer storage and run-time. The key consideration is that all the P.M. parameters are to be resolved simultaneously in a least-squares adjustment, not one P.M. magnitude at a time. Although the banded (or banded-bordered) structure of normal equations has made a ten-fold increase in the number of parameters possible with regard to a general least-squares

-5-

algorithm, even this method will fail for a much finer than 2°-resolution. Considering the current computer capabilities, a 1°- or finer resolution can be achieved, on a routine basis, only in limited areas of special interest.

A P.M. adjustment can thus be conceived in two steps. One step constitutes what has been called a second-phase adjustment built on the global first-phase adjustment. And the other step can be called a third-phase adjustment, which amounts to an additional P.M. densification in areas of special interest. In analogy to the former case, this adjustment is built on the minus geoidal residuals from the previous step, that is, from the second-phase solution. The set of point masses forms now a denser grid compared to the second phase, and the depth is commensurably smaller. The final quantities of interest are obtained through the sum of three parts, each corresponding to the appropriate phase. In this way, the transition of contour lines between the lower and the higher resolution areas is gradual. As an example of SEASAT altimetry, the second phase could be designed to model a 2°-geoid over the global oceans, and the third phase could be designed to model a 1°-geoid in the western part of the North Atlantic. Due to SEASAT tracks intersecting in an approximate $1^{o} \times 1^{o}$ equilateral grid, a resolution superior to a 1°-geoid would fail in principle due to insufficient data.

2.2 Collocation Approach

The basic difference distinguishing the collocation approach from the P.M. adjustment, from the computational point of view, is that a simultaneous least-squares adjustment of several variables does not take place. In principle, only one prediction point is solved for at a time. Accordingly, instead of an inversion of a large, albeit strongly patterned system of normal equations, inversions of small matrices take place, one inversion per prediction point. The prediction points themselves can be distributed in an equilateral grid similar (or identical) to the P.M. grid considered previously. In this case the resolution power, corresponding to an (n',n') S.H. expansion, is similar in both approaches. Consistent with this concept, the realization of the (n',n') geoid in the adapted collocation approach entails pushing the higher-resolution features (with respect to the n',n' S.H. expansion) into the realm of "noise".

The (new) observations are again minus the geoidal residuals from the first phase, and they can again be limited to those located within a given spherical cap from the desired prediction point. The predictions of greatest interest are those of geoid undulations, obtained through the use of the geoidal covariance function; predictions of other quantities such as gravity anomalies can be obtained for the same location upon using the appropriate cross-covariance function. All the predicted quantities refer to the "normal field" represented by an (n,n) S.H. expansion, where $n=14$ has usually been chosen.

Since the number of observations involved with one prediction point can be made reasonably small (see, e.g., weighted averaging of observations located close together, as explained in Section 6.4 of [Blaha, 1984]), one is faced with inverting N small matrices as opposed to inverting an N×N system of normal equations, where N is the number of prediction points. This allows for modest

-7-

computer storage requirements which are set to accommodate, in one "loop", a
chosen number of prediction points together with the corresponding vectors and
matrices of small dimensions. Since the prediction procedure applies to one
point at a time, predictions in subsequent "loops" can be made (and stored on a
magnetic tape) for the whole oceanic geoid essentially in an arbitrarily dense
grid.

The predictions of the (n',n') geoid based on the (n,n) "normal field" can
be made with advantage in the original equilateral grid of prediction points,
rather than in a finer grid. The original grid can later be densified at will
upon using the economical "errorless collocation". Such a procedure utilizes
the original predictions in the role of observations and computes the pertinent
matrices (M^T and H in [Blaha, 1984]) with the value n', rather than infinity,
implying that the expansion of the covariance function ends with n' and that the
geoid beyond (n',n') is considered to be "zero".

The densified grid corresponding to the (n',n') S.H. expansion can be used
for a variety of purposes. For example, it can serve during the construction of
a geoidal contour map (in this case it may be useful to make it a fairly dense
geographical grid). In a very similar procedure, the original as well as the
densified grid can be made to represent other geophysical quantities besides
geoid undulations, such as gravity anomalies. As another example, an equilateral
densified grid can serve in the computation of S.H. potential coefficients, via
integral formulas, through the degree and order (n',n'). A lower degree and
order expansion, if desired, can be obtained simply by a truncation of the
expansion just formulated, due to the familiar orthogonality properties of spheri-
cal harmonics. As will transpire in later chapters, the original equilateral
grid of prediction points may in itself be sufficient for such a determination
of S.H. potential coefficients.

-8-

In analogy to the P.M. approach, a third-phase collocation solution can be built on the results (minus the geoidal residuals) of a second-phase solution; in this case, n of the "reference field" should be replaced by n'. The final quantities of interest are again obtained as the sum of three parts, etc. However, due to the practical feature of solving for one prediction point at a time, such a detailed gravity field representation could be obtained on a global scale already in the second phase if desired. By comparison, in the P.M. approach the necessity to produce a medium-detail resolution in the second-phase adjustment was dictated by the fact that the most detailed solution would be impossible to obtain on a global scale, and that some global solution is always desired.

However, the option of readjusting certain tidal effects (tidal amplitudes and phase angles for selected tidal constituents) is not available in the collocation approach. Such a readjustment can be made in individual ocean basins in the second-phase P.M. adjustment. If this readjustment is desired in conjunction with a detailed description of the earth's gravity field, it could be achieved through a combination of the P.M. and the collocation approaches. In particular, one could perform a relatively coarse second-phase P.M. adjustment, followed by a collocation solution based on minus the geoidal residuals from the former. As an example, a global P.M. solution could be carried out for a $4^{\circ} \times 4^{\circ}$ equilateral grid of point masses (distributed over the world's oceans), which would also include a readjustment of the tidal amplitudes and phases for the constituents M_2, N_2 and O_1; in the case of SEASAT, the constituents S_2, K_2, K_1 and P_1 could not be properly resolved, see e.g. Chapter 5 in [Blaha, 1982]. The collocation approach could then follow with the prediction points forming a $1^{\circ} \times 1^{\circ}$ equilateral grid, and result in a 1°-global resolution.

3. ROLE OF THE POINT-MASS CONFIGURATION
IN DESCRIBING THE GRAVITY FIELD DETAIL

In [Blaha, 1983], the concept of a point-mass (P.M.) adjustment built on

minus the geoidal residuals from the global spherical-harmonic (S.H.) adjust-

ment was extended from a single- to a double-layer P.M. configuration. The

latter involves twin point masses located along the same vertical, i.e.,

along the same radius in spherical approximation, separated by a pre-determined

distance v. These twin point masses are identical in magnitude, but differ in

sign. The double-layer algorithm has been tested through a comparison with the

same adjustment problem solved by means of a single P.M. layer. The locations

of point masses in the shallower layer have been made to coincide with the

locations in the single-layer approach. As the separation v was being increased,

all the results were approaching their counterparts from the single-layer adjust-

ment. Finally, when this separation reached several earth's radii, the two sets

of results became identical. Such a "depth" of the second layer has no physical

meaning, but represents a mathematical tool in verifying the two approaches.

Another test has been performed in the double-layer P.M. mode alone upon

the assumption of linearity in the model. This assumption implies that v must

be sufficiently small with respect to the horizontal separation (s) of the

point masses and the depth (d) of the shallower layer. In this context, the

adjustment model for one observation and one twin point mass as described on

page 68 of [Blaha, 1983] reads:

$$\tilde{0}_i = (\partial C_{ij}/\partial R_1) \, v \, (kM)_j \, , \tag{3.1}$$

where $\tilde{0}_i$ is the observed quantity (considered here as geoid undulation), C_{ij}

is the coefficient of the P.M. magnitude in the single-layer mode, R_1 is the

radius from the earth's center associated with this layer, v is the separation

already defined, and $(kM)_j$ is the (scaled) magnitude of the point mass "j".

One can now consider n twin point masses grouped in the vector X, in which case

(3.1) becomes

$$\tilde{0}_i = aX , \tag{3.2a}$$

$$a = v \, a' , \tag{3.2b}$$

where the row-vector a' is associated with the separation v = unity.

In the presence of a redundant number of observations one forms the familiar

observation equations as

$$V = AX + L , \tag{3.3a}$$

where V is the vector of residuals, A is the "design" matrix composed of the rows

"a" above, X is the vector already defined (containing P.M. magnitudes as param-

eters to be determined from the adjustment), and L is the vector of constant

terms (here consisting directly of minus the observed values, due to the zero

initial values of parameters). Similar to (3.2b), one can write

$$A = v \, A' , \tag{3.3b}$$

where A' consists of rows a' described following (3.2b). The least-squares

solution for the parameters reads

$$X = -(A^T P A)^{-1} A^T P L . \tag{3.4}$$

In the case v = unity , one would similarly have

$$X' = -(A'^T P A')^{-1} A'^T P L . \tag{3.5}$$

With Σ symbolizing variance-covariance matrices, due to (3.3b) it follows that

$$X = (1/v)X' , \tag{3.6a}$$

$$\Sigma_X = (1/v^2)\Sigma_{X'} . \tag{3.6b}$$

Equation (3.6b) implies that

$$\sigma_{X_j} = (1/v)\sigma_{X'_j} . \tag{3.7}$$

These results have been verified upon comparing the outcome of a given adjustment where $s = 222$ km, $d = 175$ km, and where v has varied as $v = 500$ m, $v = 100$ m, and $v = 1$ m.

The adjusted values of observed quantities are confirmed to be

$$L^a = AX = v A' (1/v) X' = A'X' = L'^a . \tag{3.8}$$

This implies, under the assumption of small v, that the adjusted observations are invariable of v. Similar outcome is reached for adjusted linear functions of parameters:

$$\overline{L}^a = \overline{A}X = v \overline{A}' (1/v) X' = \overline{A}'X' = \overline{L}'^a. \tag{3.9}$$

Equations (3.8) and (3.9) have also been confirmed through the adjustment mentioned at the end of the last paragraph. The quantities in (3.8) were geoid undulations while the quantities in (3.9) were gravity anomalies and deflections of the vertical. In fact, selected variance-covariances of all these quantities have been verified as well. In summary, the final results (geoid undulations, gravity anomalies, etc.) as well as their variance-covariances are invariant of the (small) numerical value of v, unlike in the case of the P.M. parameters themselves, which vary in proportion to $1/v$ and whose variance-covariances vary in proportion to $1/v^2$.

-12-

After being verified in the manner described above, the double-layer P.M. algorithm has been utilized to conduct a series of tests. The purpose of these tests has been to determine what kind of influence can be exercised by the value of v (no longer small) on the fit of the adjusted P.M. geoid to the altimeter residuals from the S.H. adjustment. The measure of the fit is provided by the root mean square (r.m.s.) of the resulting, or second-phase, residuals. The oceanic area selected for these tests is near Antarctica, delimited by the parallels -68° and -44°, and by the meridians 150° and 280°. This area produced 22,819 residuals. The point masses were distributed in a $2^{\circ} \times 2^{\circ}$ equilateral grid (approximately 222 km x 222 km), extending beyond the residual area, so that s = 222 km. The number of (twin) point masses was 677. The radius of the spherical cap beyond which the observations are ignored in conjunction with a given point mass was stipulated in accordance with previous conventions as 1.5 s. The depth of the shallower layer was chosen according to the d/s ratios: 0.1/1, 0.2/1, 0.4/1, 0.6/1, 0.8/1, 1.2/1, and 1.6/1. The vertical separation between the two layers was chosen as $v \to 0$ (in practice 100 m), 0.4 d, 0.6 d, 0.9 d, 1.5 d, and $v \to \infty$. The last case amounts to performing a single-layer P.M. adjustment.

The above test cases are grouped in Table 1 featuring their r.m.s. residual. Underneath each r.m.s. value is listed in parentheses the average magnitude of the residuals (i.e., the average absolute value). The average residual in each category approaches zero and, therefore, is not listed. The largest values would be +0.04 m in the first row with the exception of 0.00 m for $v \to \infty$. In all the other cases the size of the average residual is 2 cm or less. One notices that with the exception of most cases in the categories d/s = 0.1/1 and d/s = 0.2/1 , the r.m.s. residual ranges within narrow limits, from 0.91 m to 1.00 m. This accords very well with the theoretical sigma of approximately

d/s	v→0	v=0.4d	v=0.6d	v=0.9d	v=1.5d	v→∞
0.1/1	1.22 (0.89)	1.20 (0.87)	1.20 (0.87)	1.20 (0.87)	1.14 (0.82)	0.95 (0.67)
0.2/1	1.10 (0.78)	1.05 (0.74)	1.03 (0.75)	1.01 (0.75)	0.98 (0.69)	0.95 (0.67)
0.4/1	0.94 (0.66)	0.93 (0.65)	0.92 (0.65)	0.92 (0.64)	0.92 (0.64)	0.97 (0.69)
0.6/1	0.91 (0.64)	0.91 (0.64)	0.92 (0.64)	0.92 (0.65)	0.93 (0.66)	0.98 (0.70)
0.8/1	0.92 (0.64)	0.93 (0.66)	0.94 (0.67)	0.95 (0.67)	0.96 (0.68)	0.99 (0.70)
1.2/1	0.96 (0.68)	0.97 (0.69)	0.98 (0.70)	0.98 (0.70)	0.98 (0.70)	0.99 (0.71)
1.6/1	0.98 (0.70)	0.99 (0.70)	0.99 (0.70)	0.99 (0.70)	0.99 (0.71)	1.00 (0.71)

Table 1

Results of the test cases with varying d, v; listed are r.m.s. of the residuals and, in parentheses, their average magnitude (both in meters)

one meter, obtained from the covariance function for the corresponding (90,90)
S.H. expansion. Likewise, the average magnitude ranges within narrow limits
from 0.64 m to 0.71 m.

A global P.M. adjustment has recently been performed at AFGL in the single
P.M. mode ($v \to \infty$), with d/s = 0.8/1. It follows from the above experience that
if the same adjustment were performed in the configuration d/s = 0.6/1 in con-
junction with a small or moderate value of v (between zero and 50 km or even
100 km), the r.m.s. residual would likely improve by some 7%. This improvement
is by no means substantial and might not even justify a global adjustment in the
double-layer P.M. mode which is computationally more demanding than the single-
layer mode. Indeed, the main outcome of the above tests points to rather
insignificant variations in the geoidal fit as a function of the depth of the
shallower P.M. layer (provided it is within reasonable limits) and as a function
of the separation between the two layers. This indicates that the power of the
resolution is linked almost entirely to the horizontal distribution of the point
masses.

4. REPRESENTATION OF COLLOCATION RESULTS
BY A SPHERICAL-HARMONIC EXPANSION

This chapter is concerned with designing a strategy which will lead to
compatible gravity field representations using two methods. The first method
is the modified collocation with noise as developed in [Blaha, 1984], and the
second method comprises a spherical-harmonic (S.H.) expansion. The above term
"modified" does not mean that the general concept of the least-squares collo-
cation with noise is violated in any sense. Rather, this concept is applied in
a modified situation, where the earth's gravity field is considered to be
idealized (smoothed out) in that it is exactly expressible by a S.H. expansion
complete through a desired degree and order (n',n').

The important characteristic of the second method is that the S.H. potential
coefficients are to be computed from the results of the first method, which they
should ideally reproduce. Here these coefficients will be derived from the
collocation predictions of geoid undulations. A similar procedure could, of
course, be undertaken with respect to gravity anomalies. But since the present
treatment is based on altimetric observations, the collocation predictions of
geoid undulations are more directly derived quantities than gravity anomalies
or other functions of the geopotential, and as such will be used in the analysis.

The general formulas for the least-squares collocation with noise read

$$\hat{P} = M^T(H + \Sigma)^{-1}\bar{F} , \tag{4.1a}$$

$$C_{\hat{P}} = H_P - M^T(H + \Sigma)^{-1}M , \tag{4.1b}$$

where

$\hat{P}$ = the vector of predicted quantities, here geoid undulations at the chosen prediction points,

$C_{\hat{P}}$ = the error measure of these quantities, similar in character to a variance-covariance matrix,

$\overline{F}$ = the vector of actual observations, here geoid undulations at the given observation points; it is composed of the vector F (errorless geoid undulations) and the vector e (observational noise), namely

$$\overline{F} = F + e , \qquad (4.1c)$$

Σ = the variance-covariance matrix of the observational noise, and

H, M^T, H_P = matrices formed in a standard way, here using the covariance function for geoid undulations, where H pertains to observation points, M^T to both prediction and observation points, and H_P to prediction points.

The general covariance function for geoid undulations is given by

$$D(\psi) = \sum_{k=n+1}^{\infty} d_k P_k(\cos\psi) , \qquad (4.2)$$

where n is the degree and order of the reference field, here a (14,14) field, hence n=14; it is thus apparent that the term "geoid undulations" as used above should be understood with respect to such a reference field. Further, d_k is the k-th degree variance and $P_k(\cos\psi)$ is the Legendre polynomial in the argument $\cos\psi$, where ψ is the spherical distance between the points concerned. Equation (4.2) corresponds to the actual gravity field, which could be thought of as described by an (∞,∞) S.H. expansion.

Suppose now that an idealized gravity field is exactly expressible through an (n',n') S.H. expansion; i.e., the geoid undulations corresponding to the S.H.

-17-

coefficients beyond the degree and order n' are identically zero. In such a case, the geoidal covariance function would become

$$D'(\psi) = \sum_{k=n+1}^{n'} d_k P_k(\cos\psi) \ . \tag{4.3}$$

The formulas (4.1a,b) would remain unchanged in this situation, except that the matrices H, M^T and H_p would be formed with the aid of the covariance function given by (4.3) instead of (4.2). Furthermore, the vector F (measured via Γ) would become F', composed of errorless geoid undulations associated with the S.H. expansion (n',n'), currently under consideration, instead of the expansion (∞,∞).

Next, make several temporary assumptions based on the notion just introduced:

1) the measured surface is the idealized geoid corresponding to the above gravity field (n',n');

2) the observations have an ideal global configuration, i.e., they are sufficiently dense and uniform;

3) the observations have an ideal quality, i.e., e = 0, Σ = 0;

4) the predictions are made using all of the observations in conjunction with any one prediction point;

5) the predictions have an ideal global configuration, i.e., are made in an arbitrarily dense equilateral grid.

Clearly, such assumptions are unrealistic both with regard to the observations (items 2 and 3) and to the computation of the predictions (items 4 and 5). Although the basic assumption (item 1) is unrealistic as well, it expresses an approximation of the actual gravity field by the (n',n') field, which is an important goal common to both methods. The other assumptions (items 2 - 5)

-18-

reflect an initial stage, where the two methods lead to identical results. These assumptions will eventually be relaxed, but one should keep in mind that *the gravity field representation should be consistent in the two methods.*

The first method presents the idealized geoid already as the result of item 5 above, in that a geoidal contour map can be constructed from the (dense) global predictions. On the other hand, due to the same item the S.H. potential coefficients in the second method can be computed by the integral formula

$$\begin{Bmatrix} \Delta \overline{C}_{nm} \\ \Delta \overline{S}_{nm} \end{Bmatrix} = [1/(4\pi R)] \iint_{\sigma} N \ \overline{P}_{nm}(\sin\phi) \begin{Bmatrix} \cos m\lambda \\ \sin m\lambda \end{Bmatrix} d\sigma \qquad (4.4)$$

where, on the right-hand side,

R = the earth's mean radius,

N = the geoid undulation (referring to the 14,14 reference field),

$\overline{P}_{nm}(\sin\phi)$ = the normalized Legendre functions in the argument $\sin\phi$,

ϕ, λ = the geocentric latitude and longitude, respectively, of the point associated with N , and

$d\sigma$ = the (spherical) surface element associated with N.

Due to the relatively high-degree and order reference field, the spherical approximation is inconsequential. For the same reason, one has $\Delta \overline{C}_{nm} = \overline{C}_{nm}$, while $\Delta \overline{S}_{nm} \cong \overline{S}_{nm}$, the normalized S.H. coefficients.

Upon using the S.H. potential coefficients as computed above, the second method yields the geoid undulations according to the formula which, in the present case, reads

$$N = R \sum_{k=n+1}^{n'} \sum_{\ell=0}^{k} (\Delta \overline{C}_{k\ell} \cos \ell\lambda + \Delta \overline{S}_{k\ell} \sin \ell\lambda) \ \overline{P}_{k\ell}(\sin\phi) , \qquad (4.5)$$

where ϕ,λ refer to the point associated with N. If such a point coincides with a collocation prediction point, the predicted value should be exactly reproduced by (4.5). Thus, under the above assumptions the two methods are equivalent.

Computer simulations in the next chapter will resolve the practical question regarding the density of prediction points needed for a satisfactory S.H. representation of the collocation results. In this task, the assumptions (1) - (4) are left intact, but the predictions are generated in a finite equilateral grid. For example, if n'=90, such a grid could have no more than 2.23° on the side, due to a relationship between the number of measurements and the number of unknowns. But from the standpoint of a good S.H. representation, this value should be smaller. However, an answer to the question whether a $2^\circ \times 2^\circ$ or, per-haps, a $1^\circ \times 1^\circ$ equilateral grid is necessary in this task will be obtained from computer simulations which will generate the required observations (items 2 and 3) describing the idealized geoid (item 1). In particular, one will be able to find the threshhold size beyond which the familiar orthogonality relations for spherical harmonics are disturbed in a way significantly affecting the results.

Such a threshhold can then serve in computing the S.H. potential coef-ficients using the actual altimetric observations. The remaining assumptions (items 1 - 4) are dealt with at the level of the collocation approach alone. By virtue of the relatively high-degree and order reference surface, the covariance function decreases rapidly with increasing distance, which allows the use of only those observations which are located in a relatively small spherical cap centered at a given prediction point -- not all the available observations. This consideration removes the need for the assumption of item 4 in practical terms.

The most important assumption is that of item 1. It is treated in the modified collocation approach by splitting F into F', corresponding to the (n',n') field, and F", representing the effects beyond this field. Since the actual observations sense the effects of the entire field -- not only those of the hypothetical (n',n') field -- the part F" acts as if it were augmenting the level of the noise, in the sense of adding a part of the signal to the noise. In considering (4.1c), this concept is represented by the new formula

$$\overline{F} = F' + (F'' + e) \, ,$$

where F' corresponds to the idealized geoid as just stated, and (F" + e) is the modified noise. The resulting modified collocation formulation is similar to (4.1a,b), except that the covariance function involved in the formation of the matrices M^T and H_p, but not H, is utilized in conjunction with n' (equation 4.3) instead of ∞ (equation 4.2). Of the remaining assumptions, item (2) is fulfilled reasonably well over the oceanic areas, and item (3) is inconsequential, considering the precision of satellite altimetry.

5. EVALUATION OF SPHERICAL-HARMONIC POTENTIAL COEFFICIENTS VIA INTEGRAL FORMULAS

5.1 Design of the Basic Procedure

The main topic to be addressed concerns the evaluation of spherical-harmonic potential coefficients via integral formulas, with geoid undulations as the known quantities. The emphasis on geoid undulations stems from their availability over most of the earth's surface, directly attributable to an increased exploitation of satellite altimetry. The integral formulas will be applied to discrete data sets and their acceptability will be assessed through computer simulations.

The quantities of key importance in this task consist of "errorless" geoid undulations (N) generated through the degree and order n'; the reference ellipsoid is assumed to have the same potential as the geoid and the same mass as the earth, and is centered at the earth's center of mass. In the spherical approximation, the formula used in generating geoid undulations reads

$$N = R \sum_{n=2}^{n'} \sum_{m=0}^{n} (\Delta \bar{C}_{nm} \cos m\lambda + \Delta \bar{S}_{nm} \sin m\lambda)\bar{P}_{nm}(\sin\phi) , \qquad (5.1)$$

where R is the earth's mean radius (6371 km), ϕ and λ are the geocentric latitude and longitude, respectively, $\Delta \bar{C}_{nm}$ and $\Delta \bar{S}_{nm} \equiv \Delta \bar{S}_{nm}$ are the normalized spherical-harmonic (S.H.) potential coefficients referring to the normal (ellipsoidal) field, and $\bar{P}_{nm}(\sin\phi)$ are the normalized associated Legendre functions in the argument $\sin\phi$. Due to the potential and mass assumptions, the mean value of geoid undulations is zero.

The integral formula giving the S.H. coefficients based on the knowledge
of N is written as

$$
\begin{Bmatrix} \Delta \overline{C}_{nm} \\ \Delta \overline{S}_{nm} \end{Bmatrix} = [1/(4\pi R)] \iint_{\sigma} N \ \overline{P}_{nm}(\sin\phi) \begin{Bmatrix} \cos m\lambda \\ \sin m\lambda \end{Bmatrix} d\sigma \ , \tag{5.2}
$$

where σ denotes the surface of the unit sphere and $d\sigma$ is the surface element.
This formula follows from (5.1), where the geoid undulations are regarded as
functions on a sphere and are expressed in terms of surface spherical harmonics
(see Sections 1-13 and 1-14 in [Heiskanen and Moritz, 1967]).

Suppose now that the elements $d\sigma$ are replaced by finite surface areas $d\sigma_i$,
each associated with a centrally located geoid undulation N_i. If these areas
are sufficiently small, the integration operator in (5.2) can be replaced by the
summation operator. If, moreover, all of $d\sigma_i$ have an equal area, the formula is
further simplified to read

$$
\begin{Bmatrix} \Delta \overline{C}_{nm} \\ \Delta \overline{S}_{nm} \end{Bmatrix} = (1/R)(1/P) \sum_{i=1}^{P} N_i \ \overline{P}_{nm}(\sin\phi_i) \begin{Bmatrix} \cos m\lambda_i \\ \sin m\lambda_i \end{Bmatrix} , \tag{5.3}
$$

where P is the total number of geoid undulations N_i, whose locations (points "i")
are described by the coordinates (ϕ_i, λ_i). In fact, the equal area criterion
leads to all of the N_i in (5.3) having an equal weight. Thus, in this "finite"
case, the integral formula (5.2) becomes the numerical integration formula (5.3).

For the sake of simplification in practical computations, the points "i",
i = 1, 2, ..., P, are usually desired in a regular grid. Due to the difficulty
in computing the associated Legendre functions, it is expedient to design the
grid in ϕ- and λ- coordinates to that these functions are computed only once

-23-

for a number of grid points (along the same parallel). The grid intervals in ϕ and λ are taken as

$$\Delta\phi \ , \qquad \Delta\phi/\cos\phi_i \ , \tag{5.4}$$

respectively. The surface areas $d\sigma_i$ are then considered to form geographic compartments, called blocks, whose dimensions $\Delta\phi$ and $\Delta\lambda$ are again given by (5.4), and which contain the points "i" in their geographic centers. By virtue of (5.4), the equal area requirement for the blocks is satisfied and the grid formed by the points "i" is called equilateral. Equation (5.3) can now be presented in a computationally advantageous form:

$$\left\{\begin{matrix} \Delta\overline{C}_{nm} \\ \Delta\overline{S}_{nm} \end{matrix}\right\} = (1/R)(1/P) \sum_{k=1}^{K} [\overline{P}_{nm}(\sin\phi_k) \sum_{\ell=1}^{P_k} N_{k\ell} \left\{\begin{matrix} \cos m\lambda_{k\ell} \\ \sin m\lambda_{k\ell} \end{matrix}\right\}] \ , \tag{5.5a}$$

$$P = \sum_{k=1}^{K} p_k \ , \tag{5.5b}$$

where K is the number of parallels containing grid points and p_k is the number of grid points on the parallel "k".

With the S.H. coefficients computed from (5.5a,b), one should ideally recover the errorless values of N by a new application of (5.1), whether at the grid points where N_i ($N_{k\ell}$ in the notations of 5.5a) were originally generated, or at other points. If the recovery is judged acceptable, so is the density of the grid. Otherwise, the grid is too coarse with respect to the degree and order of the desired S.H. coefficients, in the sense that the familiar orthogonal relations are no longer fulfilled in the finite case. These relations, demonstrated in Section 1-14 of [Heiskanen and Moritz, 1967], read

-24-

$$\iint_\sigma \bar{R}_{nm} \bar{R}_{sr}\, d\sigma = 0, \qquad \iint_\sigma \bar{S}_{nm} \bar{S}_{sr}\, d\sigma = 0 , \qquad \iint_\sigma \bar{R}_{nm} \bar{S}_{sr}\, d\sigma = 0 , \tag{5.6a}$$

$$\underbrace{\hspace{6cm}}_{\text{if } s \ne n \text{ or } r \ne m \text{ or both}} \qquad \underbrace{\hspace{2cm}}_{\text{in any case}}$$

$$\iint_\sigma \bar{R}_{nm}^2\, d\sigma = 4\pi , \qquad \iint_\sigma \bar{S}_{nm}^2\, d\sigma = 4\pi ; \tag{5.6b}$$

$$\begin{Bmatrix} \bar{R}_{nm} \\ \bar{S}_{nm} \end{Bmatrix} = \bar{P}_{nm}(\sin\phi) \begin{Bmatrix} \cos m\lambda \\ \sin m\lambda \end{Bmatrix} . \tag{5.6c}$$

Possible difficulties arising from the subdivision of a sphere into P compartments of finite dimensions can be assessed by exposing the connection between the equivalent formulas (5.1) and (5.2). First, (5.1) is rewritten with the notations from (5.6c) as

$$N = R \sum_{n=2}^{n'} \sum_{m=0}^{n} (\Delta\bar{C}_{nm} \bar{R}_{nm} + \Delta\bar{S}_{nm} \bar{S}_{nm}) . \tag{5.7}$$

From here it follows that

$$\tag{5.8}$$

$$\iint_\sigma N \begin{Bmatrix} \bar{R}_{sr} \\ \bar{S}_{sr} \end{Bmatrix} d\sigma = R \sum_{n=2}^{n'} \sum_{m=0}^{n} \left(\Delta\bar{C}_{nm} \iint_\sigma \bar{R}_{nm} \begin{Bmatrix} \bar{R}_{sr} \\ \bar{S}_{sr} \end{Bmatrix} d\sigma + \Delta\bar{S}_{nm} \iint_\sigma \bar{S}_{nm} \begin{Bmatrix} \bar{R}_{sr} \\ \bar{S}_{sr} \end{Bmatrix} d\sigma \right).$$

Upon considering (5.6a,b), one readily obtains

$$\iint_\sigma N \begin{Bmatrix} \bar{R}_{sr} \\ \bar{S}_{sr} \end{Bmatrix} d\sigma = 4\pi R \begin{Bmatrix} \Delta\bar{C}_{sr} \\ \Delta\bar{S}_{sr} \end{Bmatrix} . \tag{5.9}$$

Thus, equation (5.2) has been rederived, contingent precisely on the validity of all the orthogonal relations in (5.6a,b). If these relations are no longer valid due to the finite dimensions of the blocks implicated in (5.3) or (5.5a,b), the S.H. coefficients computed by the latter become distorted and, consequently, the errorless values as obtained in (5.1) with the original coefficients cannot be restored by applying this formula in conjunction with the new coefficients. The larger the blocks, the greater the distortions in the coefficients and the greater the distortions in geoid undulations (differences between the errorless and the recomputed values of N).

5.2 Initial Test Relations

The main thrust of the final analysis will be directed toward the numerical assessment of the distortions in geoid undulations. In particular, the root mean square (r.m.s.) value of these distortions will be evaluated against the background of a pre-determined standard of comparison in order to judge the grid's acceptability. However, one may wish to perform preliminary tests involving solely the errorless values N_i. The reasons may vary, such as obtaining an early indication of an improper grid design (including its density) or verifying the data-generating program and its focal point, the evaluation of the associated Legendre functions. Two kinds of tests are designed at this stage. The first, very simple test concerns the average value of N_i in conjunction with any degree of truncation (n'). And the second test concerns the r.m.s. values of N_i in two different truncations, together with the r.m.s. difference between these two sets. The results of the second test hinge again on the fulfillment of the orthogonal relations (5.6a,b) in the finite case.

The first test mentioned above is based on the familiar relations

$$\iint_\sigma \overline{R}_{nm} \, d\sigma = \iint_\sigma \overline{S}_{nm} \, d\sigma = 0 \; . \tag{5.10}$$

Accordingly, (5.7) readily yields

$$N_o \equiv (1/4\pi) \iint_\sigma N \, d\sigma = 0 \; , \tag{5.11}$$

confirming the earlier statement about the mean value of geoid undulations. In the present finite context, (5.11) corresponds to

$$\text{Ave}(N_i) \equiv (1/P) \sum_{i=1}^{P} N_i = 0 \; , \tag{5.12}$$

which has been confirmed with all the simulations performed in this study.

In view of the second test, we express the mean value of $[N(n')]^2$ and the mean value of $[N(n'')-N(n')]^2$, where the symbols (n') and (n'') indicate the degrees of truncation. Thus, $N(n')$ is given by (5.7) as it stands, while $N(n'')-N(n')$ can be written as

$$N(n'')-N(n') = R \sum_{n=n'+1}^{n''} \sum_{m=0}^{n} (\Delta \overline{C}_{nm} \overline{R}_{nm} + \Delta \overline{S}_{nm} \overline{S}_{nm}) . \qquad (5.13)$$

Since the form (5.13) differs from that of (5.7) merely by the degrees implied by the first summation, derivations involving any such expressions follow the same pattern. We now form the mean of (5.13) over the unit sphere, namely

$$(1/4\pi) \iint_{\sigma} [N(n'')-N(n')]^2 d\sigma = (1/4\pi)R^2 [\sum_{n=n'+1}^{n''} \sum_{m=0}^{n} (\Delta \overline{C}_{nm}^2 \iint_{\sigma} \overline{R}_{nm}^2 d\sigma + \Delta \overline{S}_{nm}^2 \iint_{\sigma} \overline{S}_{nm}^2 d\sigma)$$

$$+ \dots \iint_{\sigma} \text{(other products)} d\sigma] .$$

The application of (5.6a,b) yields

$$(1/4\pi) \iint_{\sigma} [N(n'')-N(n')]^2 d\sigma = R^2 \sum_{n=n'+1}^{n''} \sum_{m=0}^{n} (\Delta \overline{C}_{nm}^2 + \Delta \overline{S}_{nm}^2) . \qquad (5.14)$$

Since it can be shown (see page 91 of [Blaha, 1984]) that

$$R^2 \sum_{m=0}^{n} (\Delta \overline{C}_{nm}^2 + \Delta \overline{S}_{nm}^2) = d_n , \qquad (5.15)$$

where d_n is the n-th degree variance for geoid undulations, one can finally write

$$(1/4\pi) \iint_{\sigma} [N(n'')-N(n')]^2 d\sigma \equiv M\{[N(n'')-N(n')]^2\} = \sum_{n=n'+1}^{n''} d_n , \qquad (5.16)$$

where M designates the mean value operator. In analogy to (5.16), we also have

$$M\{[N(n')]^2\} = \sum_{n=2}^{n'} d_n \ , \qquad M\{[N(n'')]^2\} = \sum_{n=2}^{n''} d_n \ , \text{ etc.}$$

In assuming that $n' < n'' < \overline{n}$, a further application of (5.16) yields

$$M\{[N(n'')-N(n')]^2\} + M\{[N(\overline{n})-N(n'')]^2\} = M\{[N(\overline{n})-N(n')]^2\} \ , \qquad (5.17a)$$

$$\sum_{n=n'+1}^{n''} d_n \quad + \quad \sum_{n=n''+1}^{\overline{n}} d_n \quad = \quad \sum_{n=n'+1}^{\overline{n}} d_n \quad ; \qquad (5.17b)$$

the three terms in (5.17b) are the equivalent expressions of the terms directly above them.

In the finite context, the usual replacement of operators means that (5.17a) is replaced by the mean square (m.s.) relationship

$$\text{m.s.}[N(n'')-N(n')] + \text{m.s.}[N(\overline{n})-N(n'')] = \text{m.s.}[N(\overline{n})-N(n')] \ . \qquad (5.18a)$$

In the sequel, the r.m.s. values are symbolized by $\tilde{\sigma}$, so that the m.s. values can be written as $\tilde{\sigma}^2$. Furthermore, the identification of various degrees and their relationships is made via lower indices as is illustrated in the following transcription of (5.18a):

$$\tilde{\sigma}^2_{n'+1,n''} + \tilde{\sigma}^2_{n''+1,\overline{n}} = \tilde{\sigma}^2_{n'+1,\overline{n}} \ . \qquad (5.18b)$$

The usefulness of the indices transpires especially upon comparing (5.18b) with (5.17b). As has been the case several times before, the validity of the expressions such as (5.18b) hinges on the fulfillment of (5.6a,b) in the finite context.

-29-

The above discussion can be illustrated by the following example, wherein two sets of geoid undulations are generated in a $2^O \times 2^C$ equilateral grid containing 10,328 points. These sets are identified by the truncation degrees 25 and 70, implying that $n' = 2$, $n'' = 25$, and $\bar{n} = 70$. The r.m.s. values of N_i are computed as

$$\tilde{\sigma}_{2,25} = 30.2528m \ , \qquad \tilde{\sigma}_{2,70} = 30.3000m \ .$$

The differences in geoid undulations are evaluated at all the grid points, resulting in the r.m.s. value

$$\tilde{\sigma}_{26,70} = 1.6898m \ .$$

According to (5.18b), we should have

$$(\tilde{\sigma}^2_{2,25} + \tilde{\sigma}^2_{26,70})^{\frac{1}{2}} = \tilde{\sigma}_{2,70} \ . \qquad (5.19a)$$

This relation is fulfilled exactly, since

$$[(30.2528m)^2 + (1.6898m)^2]^{\frac{1}{2}} = 30.3000m \ . \qquad (5.19b)$$

In returning to the theoretical formulas (5.17a,b), except for "~" we express them through the symbolism similar to that introduced in (5.18b):

$$\sigma^2_{n'+1,n''} + \sigma^2_{n''+1,\bar{n}} = \sigma^2_{n'+1,\bar{n}} \ . \qquad (5.20a)$$

If $\bar{n} \to \infty$, the second and third symbols in (5.20a) become what is called the truncation variance, due to the truncation of an infinite series at the degrees n'' and n', respectively. One then has

$$\sigma^2_{n'+1,n''} + \sigma^2_{n''+1,\infty} = \sigma^2_{n'+1,\infty} \ . \qquad (5.20b)$$

-30-

5.3 Assessment of the Numerical Integration Algorithm

For the purpose of the present study, two equilateral grids are generated, a $2^\circ \times 2^\circ$ grid and a $4^\circ \times 4^\circ$ grid. In referring to (5.4), we have $\Delta\phi = 2^\circ$ for the first grid and $\Delta\phi = 4^\circ$ for the second grid; the intervals $\Delta\lambda$ follow from the second relation in (5.4). Theoretically, the number of square blocks (P_t) having θ on the side is $4\pi/\theta^2$; upon expressing the block side in degrees, this results in

$$P_t = (203.1^\circ/\theta^\circ)^2 . \tag{5.21}$$

Accordingly, the theoretical number of points in the above two grids is 2,578 and 10,313, respectively. Due to the rounding of the number of grid points along each parallel to the nearest integer (for safety reasons more often up than down), the actual total number (P) of the grid points used in this analysis is very slightly higher. The complete situation is summarized by

$$\theta^\circ = 2^\circ \ \ldots\ldots\ P_t = 10,313 , \quad P \approx 10,328 ; \tag{5.22a}$$

$$\theta^\circ = 4^\circ \ \ldots\ldots\ P_t = 2,578 , \quad P \approx 2,586 . \tag{5.22b}$$

It is to be noted that at both poles the blocks are replaced by spherical caps whose size is about 25% greater here.

Next, we turn our attention to the number of coefficients that can be resolved from a $\theta^\circ \times \theta^\circ$ equilateral grid of geoid undulations. In considering that θ° represents the shortest half-wavelength of the geoidal resolution expressible by an (N,N) set of S.H. coefficients, the familiar rule of thumb suggests that

$$N = 180^\circ/\theta^\circ . \tag{5.23}$$

Since the total number of coefficients in this set is $(N+1)^2$, in conjunction with the above two grids we have

$$\theta^{\circ} = 2^{\circ} \ldots (N,N) = (90,90) , \quad (N+1)^2 = 8,281 ; \qquad (5.24a)$$

$$\theta^{\circ} = 4^{\circ} \ldots (N,N) = (45,45) , \quad (N+1)^2 = 2,116 . \qquad (5.24b)$$

Upon comparing the number of data points in (5.22a,b) with the number of unknown coefficients in (5.24a,b), the former is seen to exceed the latter by 22-25%.

Suppose now that we do not wish to accept a priori the limitations (5.24a,b), and attempt to establish whether a larger set of S.H. coefficients could be resolved. In addressing this problem, we return to (5.7) and seek to solve for the S.H. coefficients as unknown parameters in a least-squares problem. Since (5.7) is linear in these coefficients, an observation equation can be formed with zero starting values for $\Delta\overline{C}_{nm}$ and $\Delta\overline{S}_{nm}$:

$$v_i = [\ldots R\overline{R}_{nm}(i) \ldots ; \ldots R\overline{S}_{nm}(i) \ldots] \begin{bmatrix} \vdots \\ \vdots \\ \Delta\overline{C}_{nm} \\ \vdots \\ --- \\ \vdots \\ \Delta\overline{S}_{nm} \\ \vdots \end{bmatrix} - N_i ,$$

where v_i is the residual, N_i is the (errorless) geoid undulation, and $\overline{R}_{nm}(i)$ and $\overline{S}_{nm}(i)$ are the functions from (5.6c), all considered at the point i with coordinates (ϕ_i, λ_i). The points i, i = 1, 2, ... , P, are again assumed to be distributed in an equilateral grid. In matrix notations, the totality of these

-32-

equations is represented by

$$V = A \, X - [N_i] \, .$$

Due to N_i having all equal weights, the regular least-squares solution is

$$X = (A^T A)^{-1} A^T [N_i] \, .$$

In the least-squares (finite) context, the consideration of crucial importance is again whether or not the orthogonal relations (5.6a,b) are reasonably well satisfied. In the affirmative, one readily confirms that the matrix of normal equations $(A^T A)$ is in theory diagonal with all the diagonal elements equal to $R^2 P$, and $A^T [N_i]$ is a vector composed of two distinct groups of elements, the first group having the form $R \Sigma N_i \overline{R}_{nm}(i)$ and the second group having the form $R \Sigma N_i \overline{S}_{nm}(i)$, where the summation Σ applies to i between 1 and P. The least-squares solution then yields

$$\left\{ \begin{array}{c} \Delta \overline{C}_{nm} \\ \Delta \overline{S}_{nm} \end{array} \right\} = (1/R)(1/P) \sum_{i=1}^{P} N_i \left\{ \begin{array}{c} \overline{R}_{nm}(i) \\ \overline{S}_{nm}(i) \end{array} \right\} ,$$

which is precisely (5.3). And in the negative, $A^T A$ can no longer be considered a diagonal matrix and the least-squares solution no longer coincides with (5.3). It would now involve the inversion of a full matrix of normal equations, and for this reason alone it is undesirable. A much more satisfactory procedure is to simply resort to a finer grid.

As we have seen earlier, a coarse grid causes the coefficients computed by (5.3) or (5.5a,b) to be distorted. The remedy is, of course, the same as above -- a finer grid. We can conclude this discussion by stating that a satisfactory solution for the S.H. coefficients is obtained when the equilateral grid used

in their evaluation is sufficiently dense, in which case the least-squares solution coincides in practice with the integrated solution (5.3) or (5.5a,b). A denser grid leads to a more perfect coincidence. We will henceforth consider only the integrated solution and judge its quality by the size of the r.m.s. distortion in geoid undulations as mentioned earlier. The least-squares analogy serves merely in searching for the largest number of S.H. coefficients one would ever consider resolving.

Clearly, if the number of observation equations were smaller than the number of parameters, a unique least-squares solution would not exist. The diagonal structure of the matrix of normal equations would be destroyed (the latter would be singular) and, accordingly, this case would be discarded. This means that the largest number of parameters we shall consider is equal to the number of grid points. If the latter is P_t, and the largest admissible set of S.H. coefficients is denoted by (N_{lim}, N_{lim}), then the limiting case we shall still examine is characterized by

$$(N_{lim} + 1)^2 = P_t .$$

In conjunction with (5.21), this implies that

$$N_{lim} = [203.1^{\circ}/\theta^{\circ} - 1]_{int} . \tag{5.25}$$

In analogy to (5.24a,b) one can now write

$$\theta^{\circ} = 2^{\circ} \dots (N_{lim}, N_{lim}) = (100, 100) , \quad (N_{lim} + 1)^2 = 10,201 ; \tag{5.26a}$$

$$\theta^{\circ} = 4^{\circ} \dots (N_{lim}, N_{lim}) = (49, 49) , \quad (N_{lim} + 1)^2 = 2,500 . \tag{5.26b}$$

Upon considering P from (5.22a,b), it is apparent that the "redundancy" has been essentially eliminated (here it amounts to merely 1-3% of the number of

coefficients). Ultimately, computer simulations will determine whether the number of coefficients in (5.26a,b), or at least that in (5.24a,b) can be satisfactorily resolved via the numerical integration (5.3) or (5.5a,b).

The computer simulations first proceed to generate errorless N_i according to (5.1) with a given set of S.H. coefficients and a chosen n', then to compute new S.H. coefficients within (n',n') via (5.5a,b), and finally to recompute N_i with the latter set of coefficients. If the r.m.s. of the distortions in N_i is smaller than the test value below, the algorithm is judged satisfactory with regard to the (n',n') set of coefficients and one can proceed to test a larger set. The same procedure applies, of course, for either grid. The test value (t) is determined under the stipulation that the r.m.s. of the distortions in N_i should increase the original truncation sigma ($\sigma_{n+1,\infty}$) by less than 5%. This occurs for

$$\text{r.m.s. (distortion)} \leq t \equiv 0.30 \ \sigma_{n'+1,\infty} \ ; \tag{5.27a}$$

in particular,

$$[\sigma^2_{n'+1,\infty} + (0.30 \ \sigma_{n'+1,\infty})^2]^{\frac{1}{2}} = 1.044 \ \sigma_{n'+1,\infty} \ , \tag{5.27b}$$

so that the increase in the truncation sigma is actually no more than 4.4%.

In order to find t needed in (5.27a), the truncation sigma is computed for various n'. A practical formula giving the latter can be transcribed from pages 62 and 63 of [Blaha, 1984] as follows:

$$\sigma^2_{n'+1,\infty} \equiv D(0) = \sum_{n=n'+1}^{\infty} d_n \ , \tag{5.28a}$$

$$d_n = 0.999617^{n+2} \ 17,981 \ m^2/[(n-1)(n-2)(n+24)] \ . \tag{5.28b}$$

As is pointed out in the above reference, these formulas can be traced to [Tscherning and Rapp, 1974]. The symbol ∞ is replaced in practice by a suitable large number, such as 1,000. Equation (5.28b) presents a close form expression for the n-th degree variance as obtained from the covariance function. A theoretical formula for the n-th degree variance based on the S.H. potential coefficients appeared as equation (5.15). The values of t computed with the aid of (5.28a,b) are listed as follows (in meters):

$$(5.29)$$

n'	14	25	40	45	49	50	70	80	90	100	110	120
$\sigma_{n'+1,\infty}(m)$	4.89	3.03	2.00	1.80	1.66	1.63	1.20	1.06	0.94	0.85	0.77	0.71
t (m)	1.47	0.91	0.60	0.54	0.50	0.49	0.36	0.32	0.28	0.25	0.23	0.21

The actual S.H. potential coefficients used in the simulations of geoid undulations are taken from a (180,180) set computed by Rapp at The Ohio State University (private communication) in 1980. In conjunction with the $2^{\circ} \times 2^{\circ}$ equilateral grid, the r.m.s. of the distortions in N_i vary according to selected degrees n' as follows:

n'	14	25	45	50	70	90	100	120
r.m.s. (m)	0.055	0.067	0.081	0.084	0.105	0.127	0.355	0.855

$$(5.30)$$

With regard to the $4^{\circ} \times 4^{\circ}$ equilateral grid, the simulations yield

n'	14	22	25	36	45	49	70
r.m.s. (m)	0.113	0.126	0.129	0.180	0.247	0.555	2.389

$$(5.31)$$

Distortions very similar to those shown in (5.30) and (5.31) have been obtained in all cases where the testing included other than grid points. In one example of this kind, geoid undulations were tested in a $4.5^{\circ} \times 4.5^{\circ}$ geographical grid, where the integrated solution of a (49,49) set of S.H. coefficients was based on the $4^{\circ} \times 4^{\circ}$ equilateral grid. Such a confirmation of the r.m.s. of the distortions is reassuring, especially when considering that the grid-point distortions in (5.31) are already deteriorating for this truncation. Thus, if non-grid points should exhibit larger distortions than the grid points, this deterioration would have certainly manifested itself in the present example chosen for its increased sensitivity.

The fact that the distortions beyond $n' = 100$ in (5.30) and beyond $n' = 49$ in (5.31) are large has been expected. These cases entail a number of S.H. coefficients larger than the number of data points, i.e., exceed the limits imposed by (5.26a,b). We also remark that when one attempts to resolve a larger set of coefficients than that utilized in generating the errorless data, the r.m.s. of the distortions starts a slight increasing trend. As one example, an errorless set (50,50) served in generating N_i in the $2^{\circ} \times 2^{\circ}$ equilateral grid. The r.m.s. of the distortions obtained with the integrated (50,50) set is listed in (5.30) as 0.084 m. But when the numerical integration proceeded through a (60,60) set, this r.m.s. increased to 0.094 m. Although the integrated values of the additional coefficients were very small (ideally they should be zero), they gave rise to a detectable deterioration in the results nonetheless. Such a deterioration appears to be less pronounced with the $2^{\circ} \times 2^{\circ}$ than with the $4^{\circ} \times 4^{\circ}$ grid. Far from being worrisome, it is consistent with the trends in (5.30,31).

In both the $2^{\circ} \times 2^{\circ}$ and $4^{\circ} \times 4^{\circ}$ equilateral grids, the r.m.s. of the distortions is somewhat smaller when computed between the latitudes $\pm 72^{\circ}$ than when computed for the whole globe. In particular, in the $2^{\circ} \times 2^{\circ}$ grid it is reduced to

approximately two-thirds of the global value for the truncations through (90,90), and in the $4° \times 4°$ grid it varies approximately from one-half to two-thirds of the global value as the truncations progress from (14,14) to (45,45). This improvement is attributed to a more regular, nearly square shape of the blocks $d\sigma_i$ closer to the equator, as opposed to the blocks near the poles and the two spherical caps at the poles themselves. However, this approximately one-third reduction in the pertinent r.m.s. values is not taken into account in the analysis, which thus might be slightly conservative.

Although the present study is concerned mainly with geoid undulations, several r.m.s. values of the distortions in gravity anomalies have also been computed. In analogy to (5.1) and (5.7), including the same assumptions, errorless values of Δg_i are first generated in an equilateral grid according to the formula

$$\Delta g = \gamma \sum_{n=2}^{n'} (n-1) \sum_{m=0}^{n} (\Delta \overline{C}_{nm} \overline{R}_{nm} + \Delta \overline{S}_{nm} \overline{S}_{nm}) \ ,$$

where γ is the average value of gravity (980 gal). We note that integral formulas giving the S.H. coefficients based on gravity anomalies could be written in analogy to (5.2) and (5.9), except that γ and Δg would replace R and N, respectively, and $1/(n-1)$ would be factored before the integral sign. The same changes would take place also with regard to the finite case (see the numerical integration 5.3 and 5.5a,b). However, this modification has not affected the present procedure where the integrated S.H. coefficients are based consistently on geoid undulations, even when used in recomputing Δg_i. This portion of the simulations has been performed only in the $2° \times 2°$ equilateral grid. The r.m.s. distortions in Δg_i have been computed in conjunction with four truncated models (n',n') as follows:

n'	50	90	100	120
r.m.s. (mgal)	0.3	1.1	4.8	13.6

$$(5.32)$$

The results (5.29) - (5.32) are the key to the main and final step in the analysis -- the determination of the applicability of the numerical integration formulas (5.3) and (5.5a,b). This determination is centered on geoid undulations in the $2^{\circ} \times 2^{\circ}$ and $4^{\circ} \times 4^{\circ}$ equilateral grids, and thus on equations (5.29) - (5.31). Equation (5.32) serves only as a peripheral confirmation of the outcome achieved with the $2^{\circ} \times 2^{\circ}$ grid. A graphic representation of the results (5.29) - (5.31) is offered in Fig. 1, where the abscissa displays the truncation degrees n', and the ordinate depicts either the values of t from (5.29) or the r.m.s. of the distortions in geoid undulations from (5.30) and (5.31). The former case (equation 5.29) is identified by the curve bearing the description "standard", and the latter two cases (equations 5.30 and 5.31) are identified by the curves bearing the descriptions "$2^{\circ} \times 2^{\circ}$" and "$4^{\circ} \times 4^{\circ}$" , respectively.

If we were to proceed strictly according to the philosophy outlined in the paragraph containing (5.27a,b), we would accept the truncation (96,96) for the $2^{\circ} \times 2^{\circ}$ grid and the truncation (48,48) for the $4^{\circ} \times 4^{\circ}$ grid as the borderline cases for the application of (5.3) and (5.5a,b). These truncations would also approach the limits in (5.26a,b), respectively. However, Fig. 1 reveals an unusual aspect conveying an important message in this respect. Both curves "$2^{\circ} \times 2^{\circ}$" and "$4^{\circ} \times 4^{\circ}$" indicate in a clearcut fashion that in this analysis, the rule embodied by (5.24a,b) is much more significant than might be expected from an approximate rule of thumb.

Indeed, in the important case "$2^{\circ} \times 2^{\circ}$" the r.m.s. of the distortions in geoid undulations through the truncation (90,90) remains comfortably low, well below the standard t in Fig. 1. Within this range, the r.m.s. increases essentially
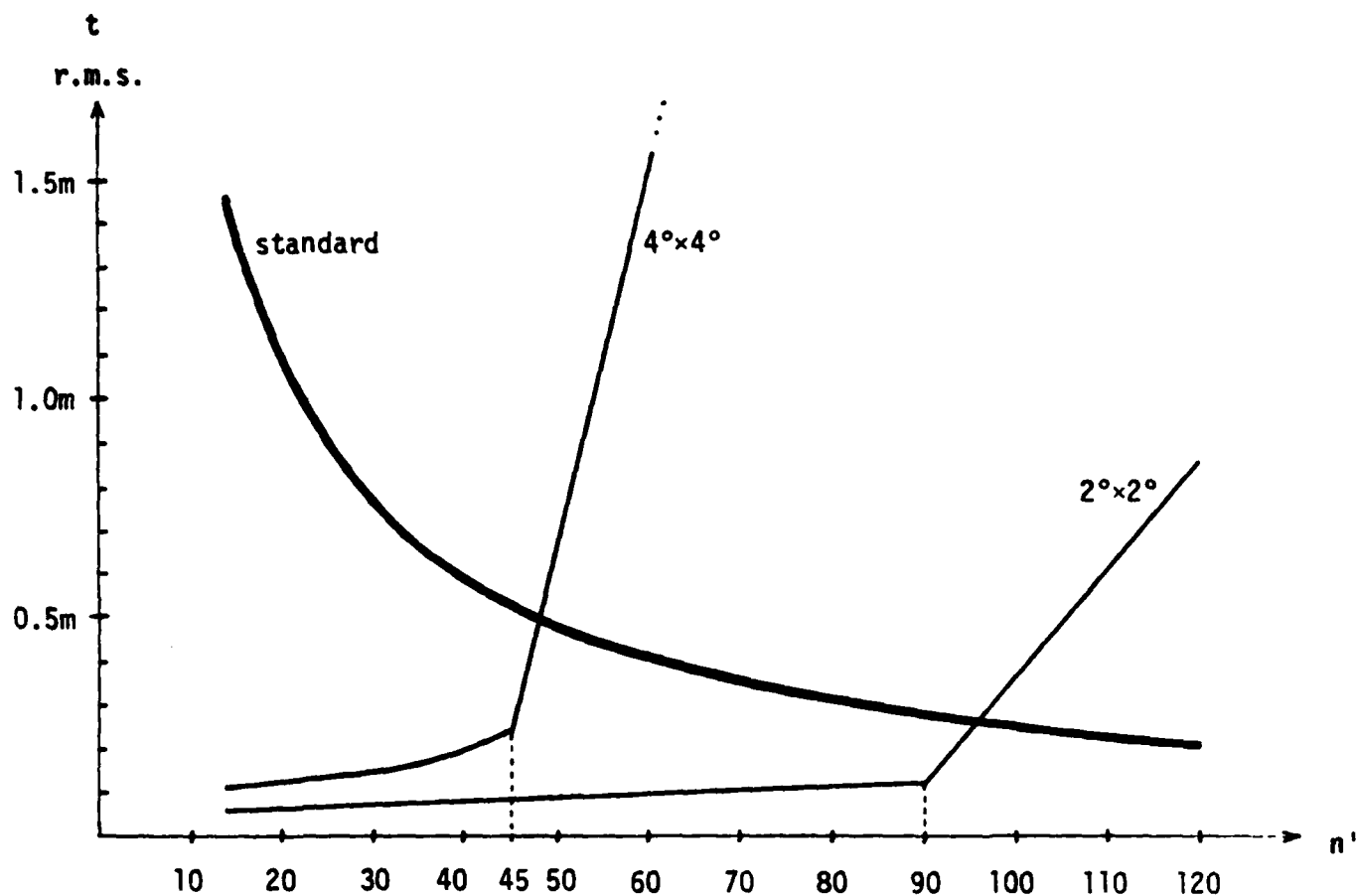
Fig. 1

Display of the curve representing the standard of comparison (t) for
different truncation degrees n', and the curves representing the r.m.s.
of the distortions in geoid undulations due to numerical integration
in 2°×2° and 4°×4° equilateral grids for different n'

in a linear fashion and at a very low rate. However, beyond the truncation (90,90) the r.m.s. deteriorates rapidly, as the figure displays in a self-evident manner. The limited analysis of the distortions in Δg summarized in (5.32) corroborates this finding. In particular, if the r.m.s. values from (5.32) were included in the figure, they would produce a pattern almost identical to that of the curve "$2^{\circ} \times 2^{\circ}$" (except, perhaps, that the slope of the deterioration beyond $n'=90$ would be slightly lower). The curve depicted as "$4^{\circ} \times 4^{\circ}$" in Fig. 1 also has clearcut characteristics, very similar, in fact, to those of the "$2^{\circ} \times 2^{\circ}$" curve. The truncation beyond which a sharp deterioration occurs is now (45,45), again demonstratively in line with the rule of thumb.

In adopting $n'=90$ in the $2^{\circ} \times 2^{\circ}$ case and $n'=45$ in the $4^{\circ} \times 4^{\circ}$ case, the r.m.s. of the distortions become 0.127 m and 0.247 m, respectively (see equations 5.30 and 5.31). These values amount to merely $0.14\sigma_{n'+1,\infty}$ in both cases (see equation 5.29). Accordingly, the increase in the original truncation sigma is not 4.4% as in (5.27b), but only 1%, since

$$[\sigma^2_{n'+1,\infty} + (0.14\ \sigma_{n'+1,\infty})^2]^{\frac{1}{2}} = 1.01\ \sigma_{n'+1,\infty} . \tag{5.33}$$

We may thus conclude that only negligibly small worsening (1%) in the original truncation sigma occurs due to the numerical integration (5.3) and (5.5a,b), provided the truncated model is (90,90) for the $2^{\circ} \times 2^{\circ}$ equilateral grid, and (45,45) for the $4^{\circ} \times 4^{\circ}$ equilateral grid.

This conclusion embodies two encouraging signs. The first points to the truncation degrees as being comfortably high, and the second, already mentioned, points to these degrees as corresponding exactly to what has been termed the rule of thumb in relating the gravity field resolution to the size of a set of S.H. potential coefficients used in the field's representation. Although this outcome has been produced with computer simulations performed in the spherical

approximation, detailed determinations of the actual gravity field can follow

the same principles and take advantage of the same computational algorithms.

Since, at AFGL, the geoid determination from satellite altimetry is based on a

(14,14) reference surface rather than an ellipsoid, the spherical approximation

entails errors on the order of a few centimeters (instead of decimeters), and is

thus deemed inconsequential.

5.4 Smoothing Effect

We have seen that the numerical integration (5.5a,b) leads to a successful modeling of geoid undulations, and thus of the disturbing potential, provided it is used up to the degree and order (N,N), where $N = 180^{\circ}/\theta^{\circ}$ according to the familiar rule of thumb presented as (5.23), in which θ° represents the side of equilateral blocks containing data points. Except for regions near the poles, the blocks are essentially square and the data points are located at their centers. The latter are conceived as forming an equilateral grid according to (5.4), where $\Delta\phi$ corresponds to θ above.

The distortions in geoid undulations (differences between the errorless and the modeled values) have been judged in the context of one and the same truncated model, i.e., in the situation where both the errorless and the modeled values are computed within the same degree and order truncation (n',n'). However, if the errorless values are generated with an "original" set (N,N) of spherical-harmonic (S.H.) coefficients, and the modeled values are computed with an integrated set (n',n'), where n'<N, the distortions owe their existence primarily to a smoothing effect. One can then judge the quality of the modeled, smoothed geoid (n',n') by comparing it with an errorless geoid (n',n') generated with the (n',n') subset of the original set of S.H. coefficients.

Ideally, the above two surfaces should coincide, i.e., the geoidal detail due to the degrees n'+1 through N should be suppressed. This desirable characteristic hinges on the fulfillment of the orthogonal reations, as can be shown in theory with the aid of (5.13). If we subject this equation to the procedure which led from (5.7) to (5.8), its right-hand side becomes zero for any $s \leq n'$ due to (5.6a). But this implies that

-43-

$$\iint_{\sigma} N(n'') \begin{Bmatrix} \overline{R}_{sr} \\ \overline{S}_{sr} \end{Bmatrix} d\sigma = \iint_{\sigma} N(n') \begin{Bmatrix} \overline{R}_{sr} \\ \overline{S}_{sr} \end{Bmatrix} d\sigma , \qquad r \leq s \leq n' \leq n'' . \qquad (5.34)$$

Therefore, when the S.H. coefficients are evaluated through the degree and order (n',n') as in (5.9), N under the integral sign can be expressible within any model (n'',n'') as long as $n'' \geq n'$. In other words, the geoidal detail described by $N(n'')-N(n')$ has no bearing on the theoretical values of the S.H. coefficients within the truncation (n',n').

Computer simulations have confirmed the above outcome in the finite case. The results presented below are sufficient to illustrate this fact. They have been obtained with the aid of a $2^{\circ} \times 2^{\circ}$ equilateral grid of geoid undulations generated via S.H. coefficients complete through the degree and order $(N,N)=(90,90)$, where N satisfies the rule (5.23). Of the models (n',n'), where the smoothing effect takes place for any $n'<N$, three are selected for a limited analysis, namely (25,25), (45,45), and (70,70).

In each of the three cases (n',n'), three values $r.m.s._i$, $i=1,2,3$, are listed:

n'	25	45	70
$r.m.s._1$ (m)	0.067	0.081	0.105
$r.m.s._2$ (m)	0.068	0.082	0.105
$r.m.s._3$ (m)	0.002	0.002	0.003

$$(5.35)$$

The first row of results, $i=1$, contains the entries from the corresponding places in (5.30) and is listed merely for the sake of comparison. The entries depict the r.m.s. of the discrepancies in geoid undulations between the (n',n') integrated values (i.e., geoid undulations computed with the n',n' set of S.H. coefficients evaluated via the numerical integration 5.5a,b) based on the (n',n') errorless values (i.e., geoid undulations $N_{k\ell}$ in 5.5a) on one hand, and the (n',n') errorless values themselves on the other hand.

-44-

The second row of results, i=2, contains the r.m.s. of the discrepancies between the (n',n') integrated values based on the (90,90) errorless values, and the (n',n') errorless values. The (n',n') integrated values in this case encompass the smoothing effect. As is apparent from this row, the smoothed (n',n') values approximate the errorless values as closely as the integrated values based directly on the smooth geoid (see the case i=1). This is strongly evidenced by the last row, i=3, depicting the r.m.s. of the differences between two kinds of (n',n') integrated values, the first based on the (n',n') errorless geoid and the second based on the (90,90) errorless geoid.

In complete analogy to (5.35), the following results are obtained with the aid of a $4^\circ \times 4^\circ$ equilateral grid of geoid undulations generated via an (N,N)=(45,45) set of S.H. coefficients where the models (n',n') are selected as (14,14), (25,25), and (36,36):

n'	14	25	36
r.m.s.$_1$ (m)	0.113	0.129	0.180
r.m.s.$_2$ (m)	0.113	0.130	0.181
r.m.s.$_3$ (m)	0.004	0.005	0.010

(5.36)

The row i=1 contains the corresponding entries from (5.31), pertaining to the differences between the (n',n') integrated values based on the (n',n') errorless values, and the (n',n') errorless values themselves. The row i=2 pertains to the differences between the (n',n') integrated values based on the (45,45) errorless values, and the (n',n') errorless values. And the row i=3 pertains to the differences between the above two kinds of (n',n') integrated values.

The results in (5.36) follow a very similar pattern to those in (5.35). In comparing the corresponding cases (25,25), one notices that all three entries in (5.36) are approximately the double of their counterparts in (5.35). This tendency can be observed already in (5.31) versus (5.30) for relatively low truncation degrees n', including the truncation (30,30) for which the respective r.m.s. values would be approximately 0.071 m and 0.152 m. Clearly, this one-half reduction in the discrepancy values is imputable to the two-fold increase in density of the equilateral grid along each dimension.

One important conclusion of this analysis consists in the finding that the portion (5.6a) of the orthogonal relations is satisfied particularly well with the selected truncation degrees n'<N, quite representative of realistic levels of smoothing. Indeed, the small magnitude of the values in the last rows of (5.35) and (5.36) indicates that the effect of geoid undulations due to the degrees n'+1 through N is almost perfectly suppressed in the application of the numerical integration algorithm.

6. APPLICATIONS OF THE NUMERICAL INTEGRATION ALGORITHM

6.1 Global Representation of the Gravity Field

A high degree and order S.H. expansion of the disturbing potential provides for a detailed representation of the earth's gravity field and its fundamental surface, the geoid. If the reference field is defined through a S.H. expansion of degree and order substantially higher than two (which corresponds essentially to an ellipsoidal field), the spherical approximation is acceptable. Thus, when referring to this field, geoid undulations and other functions of the geopotential (gravity anomalies, deflections of the vertical, etc.) can be regarded as functions on a sphere and expressed in terms of surface spherical harmonics. This has been the case at AFGL, where the global first-phase altimeter adjustment has determined a (14,14) reference field as a basis for subsequent representations of the gravity field detail, especially the oceanic geoid.

As we have seen in Chapter 5, if geoid undulations are supplied in a sufficiently dense equilateral grid all over the globe, the numerical integration algorithm permits a direct evaluation of the desired S.H. potential coefficients in the context of the above spherical approximation. This set can serve in predicting the desired geophysical quantities (especially the geoid undulations themselves) at any location. The prediction grid needed for the construction of contour maps can then be made geographic and can be densified at will.

One major source of geoid undulations distributed in an equilateral grid over the world's oceans is the modified collocation with noise, whose main features were recapitulated in Chapter 4. The grid density determines the largest size (N,N) of the set of S.H. coefficients which can be satisfactorily resolved via numerical integration (5.5a,b). This relationship was demonstrated

in Section 5.3, resulting in the confirmation of the familiar rule of thumb (5.23). Thus, a $2^O \times 2^O$ equilateral grid of geoid undulations allows for a reliable evaluation of a (90,90) set of S.H. coefficients. The same grid can *be used in expressing a smoother version of the gravity field simply by trunca-* ting the (90,90) set at a lower degree and order.

In applying the numerical integration algorithm, geoidal values over the continents must also be given. The most expedient procedure is to simulate them using some a priori set of S.H. potential coefficients complete through the required degree and order (e.g., a 90,90 set as above). This set need not be of high accuracy, since the most important product of satellite altimetry is the determination of the oceanic geoid; the contours over the land masses can ulti- mately be disregarded. On the other hand, the simulated values must be realistic (including the appropriate geoidal roughness) because otherwise the oceanic con- tours within some distance from the coasts would be deformed. We can conclude by stating that the oceanic geoid expressed by the new, integrated set of S.H. coefficients represents an improvement over that expressed by the a priori set not benefiting from the contribution of altimeter data.

6.2 Global Representation of Tidal Effects

A global tidal adjustment within the first-phase adjustment of satellite
altimetry (including S.H. potential coefficients as parameters) was described
in [Blaha, 1982] and Chapter 3 of [Blaha, 1984]. Subsequently, an optional
tidal (re)adjustment within the second-phase, large-area adjustment of satellite
altimetry (including point-mass magnitudes as parameters) was described in
Chapter 5 of [Blaha, 1984]. Since, in the second phase, the coefficients of
tidal parameters in the observation equations are adopted from the first phase,
the second-phase adjustment will no longer be mentioned in this analysis.

The a priori tidal information in the first-phase adjustment at AFGL has
been supplied via S.H. tidal coefficients. Since the Legendre polynomials and
the associated Legendre functions as well as the multiple-angle trigonometric
functions in this adjustment are computed within an (n',n') S.H. model even
without tidal considerations, little additional effort is needed when the a priori
tidal effects are expressed by a S.H. expansion within the same, or lower, degree
and order truncation. In recent adjustments of satellite altimetry, the S.H.
expansion in the first phase has been performed in a (14,14) truncated model.
On the other hand, the information pertaining to seven diurnal and semidiurnal
tidal constituents has been included via S.H. tidal coefficients in two (12,12)
sets per constituent, as is described in [Blaha, 1982] in conjunction with
[Estes, 1980].

However, much more complete (in terms of a dense global coverage) and more
accurate tidal information has become recently available in various NSWC Techni-
cal Reports by E. W. Schwiderski. The relative accuracy for each ocean-tide
constituent treated is stated to be 5 cm in the open oceans. The tidal amplitudes
and Greenwich phase angles of these constituents are tabulated in a $1^{\circ} \times 1^{\circ}$

geographical grid for all the oceanic areas in the world, and this information is also available in the form of global corange and cotidal maps. Such knowledge allows one to compute the ocean tide as a function of time and location, constituting a stepping stone in the computation of the surface tide directly related to altimeter measurements (see, e.g., Chapter 3 of [Blaha, 1984]).

The ocean-tide information for each tidal constituent can be obtained from the NSWC reports as just mentioned, or, less directly, from the S.H. tidal coefficients generated in turn from the information contained in these reports. Since the present procedure at AFGL allows for an actual adjustment of tidal amplitudes and Greenwich phase angles as parameters, provided the tidal information is supplied via S.H. tidal coefficients, the latter approach offers certain advantages. In particular, it permits an analysis of how well the tidal information is consistent with satellite altimeter observations (one could judge by the corrections attributed to the tidal parameters by the adjustment versus the a priori sigmas, etc.). Such an analysis can indicate possible weaknesses in the tidal information, the presence of systematic orbital errors of tidal frequencies, etc.

The algorithm for computing the ocean tide based on the information contained in the NSWC reports is presented as follows. First, we recapitulate the basic formulas pertaining to a constituent "j" from pages 48 and 49 in [Blaha, 1982], omitting the subscript j:

$$\xi = \xi_1 + \xi_2 , \tag{6.1a}$$

$$\xi_1 = \cos\alpha \; A \cos\psi , \quad \xi_2 = \sin\alpha \; A \sin\psi , \tag{6.1b}$$

where

$\xi \equiv \xi(\phi,\lambda,t)$ = ocean tide,

$\alpha \equiv \alpha(t)$ = Greenwich argument,

$A \equiv A(\phi,\lambda)$ = tidal amplitude,

$\psi \equiv \psi(\phi,\lambda)$ = Greenwich phase angle,

and where

ϕ,λ = geocentric latitude and longitude,

t = time.

Next, we form F and G, regarded as functions on a sphere, such that

$F \equiv F(\phi,\lambda) = A(\phi,\lambda) \cos\psi(\phi,\lambda)$,

$G \equiv G(\phi,\lambda) = A(\phi,\lambda) \sin\psi(\phi,\lambda)$.

In expressing these functions in terms of surface spherical harmonics, we have

$$F \equiv A \cos\psi = \sum_{n=0}^{\infty} \sum_{m=0}^{n} (\bar{a}_{nm}\cos m\lambda + \bar{b}_{nm}\sin m\lambda)\bar{P}_{nm}(\sin\phi) , \qquad (6.2a)$$

$$G \equiv A \sin\psi = \sum_{n=0}^{\infty} \sum_{m=0}^{n} (\bar{c}_{nm}\cos m\lambda + \bar{d}_{nm}\sin m\lambda)\bar{P}_{nm}(\sin\phi) . \qquad (6.2b)$$

The tidal amplitudes A (in cm) and Greenwich phase angles ψ (in deg.) are available from the NSWC reports. For example, [Schwiderski, 1979] presents these values for the semidiurnal principal lunar tide M_2. One can thus form F and G on the left-hand sides of (6.2a,b) for any oceanic point by finding its A on the corange map (or in the appropriate table of ocean tide amplitudes) and its ψ on the cotidal map (or in the corresponding table of ocean tide Greenwich phases).

-51-

In order to obtain the S.H. tidal coefficients $\bar{a}_{nm}$, $\bar{b}_{nm}$, $\bar{c}_{nm}$, and $\bar{d}_{nm}$ via integral formulas presented below, the values of F and G must be known (in an equilateral grid) over the whole globe, not just over the oceanic areas. Similar to the previous section, values associated with the land masses must be supplied in some manner. Stipulating unrealistic values, such as zeros, would be harmful to the tidal representation in the coastal regions.

This problem can be solved as follows. First, similar to the approach of Chapter 5 (treating N as point values) we compute the point values of the functions F and G over the oceanic areas in a suitable equilateral grid consistent with the desired degree and order truncation (n',n'). As an example, a $4^0 \times 4^0$ equilateral grid might be sufficiently dense because these coefficients would seldom be needed beyond the (45,45) truncation. Lowering the degree and order of the truncation from this level would amount to further smoothing of the information contained in the NSWC reports.

Next, we draw contours depicting the functions F and G, completing them visually over the land masses in a manner compatible with the oceanic contours. The land values of F and G have no physical meaning, and no use of their own, other than to make possible an evaluation of S.H. tidal coefficients. The latter will serve to reproduce the oceanic values and will never be used in conjunction with any point over land.

Finally, having the functions F and G in (6.2a,b) available in an equilateral grid, we proceed to the evaluation of the desired S.H. tidal coefficients in analogy to (5.5a,b):

$$\left\{ \begin{array}{c} \overline{a}_{nm} \\ \overline{b}_{nm} \end{array} \right\} = (1/P) \sum_{k=1}^{K} [\overline{P}_{nm}(\sin\phi_k) \sum_{\ell=1}^{p_k} F_{k\ell} \left\{ \begin{array}{c} \cos m\lambda_{k\ell} \\ \sin m\lambda_{k\ell} \end{array} \right\}] , \qquad (6.3a)$$

$$\left\{ \begin{array}{c} \overline{c}_{nm} \\ \overline{d}_{nm} \end{array} \right\} = (1/P) \sum_{k=1}^{K} [\overline{P}_{nm}(\sin\phi_k) \sum_{\ell=1}^{p_k} G_{k\ell} \left\{ \begin{array}{c} \cos m\lambda_{k\ell} \\ \sin m\lambda_{k\ell} \end{array} \right\}] , \qquad (6.3b)$$

$$P = \sum_{k=1}^{K} p_k , \qquad (6.3c)$$

where K is again the number of parallels containing grid points and p_k is the number of grid points on the parallel "k". Since (6.3b) differs from (6.3a) merely in the value G replacing F for each point of the (common) grid, these two relations are evaluated simultaneously.

The resulting set (n',n') of S.H. tidal coefficients can now be used in (6.2a,b), where the symbol ∞ is replaced by n', in order to recompute the functions F and G at the grid points (for verification purposes), as well as to evaluate them at any other locations. Most important in this respect are points in the oceanic regions containing altimeter data. In utilizing (6.2a,b) in (6.1a,b), the ocean tide for the pertinent constituent can be expressed as

$$\zeta = \cos\alpha \sum_{n=0}^{n'} \sum_{m=0}^{n} (\overline{a}_{nm} \cos m\lambda + \overline{b}_{nm} \sin m\lambda) \overline{P}_{nm}(\sin\phi)$$

$$+ \sin\alpha \sum_{n=0}^{n'} \sum_{m=0}^{n} (\overline{c}_{nm} \cos m\lambda + \overline{d}_{nm} \sin m\lambda) \overline{P}_{nm}(\sin\phi) . \qquad (6.4)$$

Such values of the ocean tide for the constituent "j", improved by comparison to the previous procedure, can serve in the tidal adjustment exactly as ξ_j did in [Blaha, 1982] in conjunction with Chapter 3 of [Blaha, 1984].

-53-

7. CONCLUSIONS

Two second-phase techniques have been developed in recent years at AFGL
based on the results of the global spherical-harmonic (S.H.) treatment of alti-
metric data. One of these techniques has been documented as the point-mass
(P.M.) adjustment, and the other has been described under the name of modified
collocation with noise. The former is characterized by a simultaneous adjustment
of all the P.M. parameters; however, the matrix of normal equations to be in-
verted can be made banded or, in the presence of (optional) tidal parameters,
banded-bordered. And the latter is noted for its economical property of avoiding
an inversion of a large matrix (such as is performed in the P.M. adjustment),
proceeding instead to the inversion of a number of relatively small matrices, one
per observation point; there is no limit to the number of these points. The term
"modified" attributed to the collocation technique does not concern the philos-
ophy of the least-squares collocation with noise per se, but, rather, its specific
application aimed at describing a smoothed-out gravity field, in which the part of
the signal beyond the desired smoothing level is pushed into the realm of "noise".

The P.M. adjustment has been designed in two versions, the single-layer mode,
where all the point masses are situated at one depth below the surface of the
reference ellipsoid, and the double-layer mode, where to each such point mass is
attributed another one below it, separated from it by the same vertical distance
v. The number of parameters in the latter adjustment setup is unchanged from the
former, due to the stipulation that the twin point masses differ only in sign,
not in magnitude. Even so, the double-layer mode is more time-consuming because
of an increased number of computer operations needed in the formation of observa-
tion equations.

From the tests conducted in Chapter 3 it transpires that in some cases
the double-layer adjustment may accommodate the observations (taken as minus
the geoidal residuals from the global S.H. adjustment) slightly better than its
single-layer counterpart. However, the differences are small and the improve-
ments (in terms of the r.m.s. values) do not exceed 7% for any choice of v.
Since variations in the depth of the shallower layer itself are also shown to
have only a small effect on the resulting r.m.s. of the residuals, it follows
that the power of the resolution is linked almost entirely to the horizontal dis-
tribution of the point masses. It can be concluded that due to its economic
superiority, the single-layer mode is preferable to its double-layer counterpart,
especially if the P.M. adjustment should be performed on the global oceanic scale.

If a very detailed gravity field resolution is needed in areas of special
interest, one is compelled to consider an additional treatment of altimeter data,
such as a third-phase P.M. adjustment. An adjustment of this type is the topic
of Chapter 2. It is based on the second-phase results in much the same way as the
second-phase P.M. approach is based on the outcome of the first-phase (S.H.)
adjustment. In the third phase, the point masses in an individual area of interest
form a substantially denser, and commensurably shallower grid than that character-
izing the underlying second-phase P.M. adjustment. The final quantities are ob-
tained as the sum of three parts, each corresponding to the appropriate adjustment
phase. These quantities can subsequently be used in the construction of contour
maps representing the geoid and other functions of the geopotential (such as
gravity anomalies or deflections of the vertical). In basing one adjustment
phase on the residuals from the previous phase, the concept of point masses
ensures a gradual transition of contour lines between the lower and the higher
resolution areas.

The same chapter also addresses a third-phase solution based on the second-phase results in terms of the modified collocation with noise. Except for changes at the algorithmic level, such a procedure is governed by the same principles as the third-phase versus the second-phase P.M. approach. As an example of the algorithmic changes, the (n,n) S.H. model used in the second phase as "reference field" is replaced by an (n',n') model in the third phase, which is precisely the model obtained as a solution of the second phase. Accordingly, the covariance and cross-covariance functions in the third phase exhibit sharper, more localized characteristics compared to their counterparts in the second phase.

Since the collocation approach does not provide for adjustment of tidal parameters, the third-phase collocation solution could be combined with the second-phase P.M. adjustment including tidal effects. In this way, advantages of both methods would be allowed to manifest themselves. The second phase, carried out with a relatively sparse grid of point masses, would offer the benefit of tidal adjustment at the level of individual ocean basins, while the third phase, performed in the collocation mode, would produce a detailed resolution of the gravity field on a desired scale, an ocean-basin or even a global scale.

Due to a similarity between the surface spherical-harmonic expansion of the ocean tide for a constituent "j" and the expansion of the geoid undulation, one could express the former in terms of "tidal" point masses, just as the latter has been expressed in terms of "regular" point masses. This possibility is explored in Appendix 2. A practical procedure which would treat the new P.M. parameters together with the existing ones faces one substantial difficulty -- the computer core limitations. In particular, if the present P.M. adjustment should include tidal point masses, their number would have to be small and, therefore, their distribution sparse, to the point of being equivalent to a

-56-

(22,22) S.H. expansion. Such a resolution power is only slightly better than that provided by the existing capability of the first-phase adjustment alone, although the latter affects only two parameters per tidal constituent (the tidal amplitude and the Greenwich phase angle). However, these parameters have a clearcut physical meaning and a number of advantages, as is discussed in Section 2.1 of [Blaha, 1983]. Be that as it may, the resolution power per se is not affected by a particular mode of tidal adjustment.

The present second-phase P.M. adjustment allows for a supplementary tidal adjustment of the same two parameters per constituent as discussed above. The adjustment corrections apply to the tidal effects in predetermined regions, typically in individual ocean basins, and, similar to the first phase, lend themselves readily to a physical interpretation. It is especially noteworthy that the three tidal constituents M_2, N_2, and O_1 considered in view of SEASAT altimetry add only a negligible computational burden to the adjustment process by bringing six parameters into the border of normal equations; their solution is carried out efficiently by the algorithm presented in Chapter 5 of [Blaha 1984]. This property is important when the computer core is already utilized to its capacity, and leads to the conclusion that the computer limitations make it impractical, at the present, to replace the supplementary tidal adjustment within the second-phase P.M. approach by a new procedure introducing a number of tidal P.M. parameters into the adjustment. However, an algorithm to this effect is developed in Appendix 2, which can be put to use when permitted by computational and economic factors.

In the past treatment of satellite altimetry, the first- and even the second-phase adjustment exhibited large negative altimeter residuals in areas where satellite arcs cross an important trench, such as the Puerto Rico trench. Thus, altimeter residuals may have a significant role to play in the detection of

bathymetric and other oceanic anomalies (e.g., geomagnetic anomalies). This topic is discussed at length in Appendix 3. Since it appears that a second-phase approach would be insufficient for a reliable detection of even some important trenches, and a third-phase approach would represent a lengthy and uneconomical undertaking for this purpose, one is well advised to turn to the first-phase residuals as a basic tool of such an endeavor. However, instead of considering only the actual residuals at observation points selected at $\frac{1}{4}^{\circ}$- or $\frac{1}{2}^{\circ}$-intervals in the first-phase adjustment of SEASAT altimetry (in which they allow for ample redundancy with respect to the ground-track configuration), it is now necessary to examine all the altimeter measurements in the original observational intervals of approximately 2'.

The most important part of the design, then, resides in filling in the residuals at every data location. This task can be accomplished efficiently upon undertaking a new iteration in the S.H. adjustment process, but this time utilizing all the altimeter observations and limiting the iteration merely to the computation of constant terms in the observation equations. These terms are the desired high-density and high-resolution residuals along satellite profiles. They are subsequently judged against the yardstick provided by the "truncation sigma" of the underlying S.H. model, i.e., the square root of the variance owing its existence to the truncation of theoretically infinite series. As an example, a sea surface dip larger than two or three truncation sigmas is unlikely to reflect the usual geoidal roughness, and may instead indicate the proximity of an important trench. Tests in areas of known bathymetric features, especially deep trenches, constitute a useful tool in a "fine-tuning" of such a detection procedure.

An extensive portion of the present research has been devoted to attaining a detailed S.H. representation of the earth's gravity field from a discrete set

of data. The quantities analyzed most thoroughly in this context are the geoid undulations, directly related to the disturbing potential through the familiar Bruns formula. The points of known geoid undulations (and, in several instances, gravity anomalies) are considered here to form an equilateral grid. The main task consists in finding the highest degree and order S.H. model, (N,N), which can still accurately represent the gravity field as described by the discrete data.

This task is addressed through computer simulations taking advantage of the spherical approximation. As a first step, "errorless" geoid undulations are generated with given S.H. coefficients in two equilateral grids, referred to as the $2^{\circ} \times 2^{\circ}$ and the $4^{\circ} \times 4^{\circ}$ grid. The notation $\theta^{\circ} \times \theta^{\circ}$ implies that most of the grid lines (except near, and at, the poles) give rise to squares with θ° on the side. The data generating process hinges on an algorithm able to produce accurate values of Legendre polynomials and associated Legendre function to a sufficiently high degree and order. One such algorithm, extensively tested through a (160,160) truncated model, is described in Appendix 1. It is based on recurrent relationships, and its fundamental feature resides in utilizing two starting values for each order of the associated Legendre functions, similar to the strategy customarily used for Legendre polynomials. A great increase in accuracy compared to an approach where two starting values are used to generate the entire set of these functions is well worth the additional effort.

Under certain conditions, numerical integration involving errorless data leads to the S.H. coefficients which can satisfactorily reproduce these data at the grid locations as well as at other points, whether in their original form (here geoid undulations) or in a parent form (here gravity anomalies). The theoretical development of such a procedure, together with all the pertinent computer results and tests, are presented in Chapter 5. The key element in this

analysis is the numerical integration algorithm formulated in equations (5.5a,b).

There is no need to recapitulate much of the material of Chapter 5 which is straightforward and self-contained. Its most important outcome is represented by Fig. 1, depicting the errors associated with the numerical integration of geoid undulations in the above $2^{\circ} \times 2^{\circ}$ and $4^{\circ} \times 4^{\circ}$ equilateral grids. An error measure is provided by the r.m.s. of the differences between the errorless values generated with a given (n',n') set of S.H. coefficients and the values obtained via the integrated coefficients complete to within the same set. The results are so revealing and clearcut that the curve marked "standard" in the figure becomes unnecessary. This curve symbolizes the values "t" against which the quality of the S.H. representation was to be tested.

Due to the sharp upturns in both of the "$2^{\circ} \times 2^{\circ}$" and "$4^{\circ} \times 4^{\circ}$" curves, occurring before the latter intersect the "standard" curve, the final truncations are established to the left of the corresponding intersections. Thus, the final outcome points to the (90,90) truncation in the case of the $2^{\circ} \times 2^{\circ}$ equilateral grid, and to the (45,45) truncation in the case of the $4^{\circ} \times 4^{\circ}$ grid, exactly as stipulated by the familiar rule of thumb,

$$N = 180^{\circ}/\theta^{\circ} .$$

Clearly, the importance of this rule is heightened in this concrete, tangible context.

The various truncations (n',n') examined in Chapter 5 in conjunction with the two equilateral grids reveal special properties worth further elaboration. As Fig. 1 indicates, the "$2^{\circ} \times 2^{\circ}$" curve is effectively a straight line up to the truncation (n',n')=(90,90), at which point it abruptly changes direction and continues again as a straight line, but at a much greater slope. For the sake

of interest, it can be mentioned that a curve pertaining to gravity anomalies, if plotted, would exhibit almost identical features. The "$4^{\circ} \times 4^{\circ}$" curve, whose turning point is $(n',n')=(45,45)$, behaves in a similar fashion, although its lower portion departs somewhat from a straight line for n' between 30 and 45. One can also observe from the figure that the r.m.s. of the discrepancies in the $2^{\circ} \times 2^{\circ}$ case is approximately one-half of that in the $4^{\circ} \times 4^{\circ}$ case, at least up to $n'=30$. This improvement is imputable to the two-fold increase in density, along either dimension, of the former grid with respect to the latter.

As is apparent already from Fig. 1, the final truncation values $(N,N)=(90,90)$ and $(N,N)=(45,45)$ presented above, and any truncations below such levels, lead to a very satisfactory reproduction of the errorless geoid undulations. This conclusion can be illustrated quantitatively upon combining (in the quadratic sense) the original truncation sigma with the r.m.s. of the discrepancies due to the numerical integration algorithm, and obtaining a "new" truncation sigma for geoid undulations. In either of the two cases under consideration, the truncation sigma is seen to increase by a mere 1% -- an encouraging sign indeed.

The outcome of Chapter 5 can be effectively exploited in representing collocation results in terms of the S.H. expansion of the geopotential. This topic is treated in Chapter 4 and the first section of Chapter 6. For example, a $2^{\circ} \times 2^{\circ}$ equilateral grid of geoid undulations predicted through the modified collocation with noise at the smoothing level $(n',n')=(90,90)$ can be utilized to produce an integrated (90,90) set of S.H. coefficients consistent with the collocation results. Since the emphasis in the final representation is on the oceanic geoid, the (missing) prediction values over land can be filled in with a lesser accuracy, upon using an a priori set of S.H. potential coefficients truncated at the same level.

-61-

Finally, the second section of Chapter 6 addresses the problem of using a S.H. expansion in representing the desired tidal effects. These effects are described in detail, and to a high level of accuracy, by E. W. Schwiderski in his NSWC Technical Reports. Each tidal constituent considered involves two sets of S.H. tidal coefficients. Some of the principles presented in Chapter 5 are utilized here as well, especially the numerical integration algorithm recapitulated as (6.3a-c). This algorithm is used in conjunction with an equilateral grid of functions called F and G, evaluated over water with the aid of the above NSWC reports and over land via visual interpolation.

If this grid is chosen as $4^{o} \times 4^{o}$, the earlier rule of thumb allows for a reliable reproduction of the functions F and G through a (45,45) set of integrated S.H. tidal coefficients. A lower degree and order set can also be used in practice, implying further smoothing of the NSWC information (in the above reports, the tidal information is available in a $1^{o} \times 1^{o}$ geographical grid). Finally, the ocean tide for a desired constituent "j" can be expressed as in (6.4), and can serve in the tidal adjustment in exactly the same manner as its former counterpart did in [Blaha, 1982] and Chapter 3 of [Blaha, 1984].

APPENDIX 1
DEVELOPMENT OF A RECURRENT ALGORITHM
FOR LEGENDRE POLYNOMIALS AND ASSOCIATED LEGENDRE FUNCTIONS

This Appendix describes in detail the algorithm developed and tested during the period July 1 - September 30, 1982, and presented in Status Report No. 3 for the same period. A similar algorithm was summarized in September, 1982 by Rapp [1982], pages 9 and 10. There are a few minor differences between the two approaches, however. For example, here the recurrent relationships are derived in terms of the quantities $\overline{P}_n^{[m]}$ rather than $\overline{P}_{nm}$. The derivations in this Appendix are presented against the AFGL background including earlier versions, and have thus a somewhat tutorial character.

In the past, geoid undulations and other geophysical quantities were computed at AFGL on a global scale using the conventional spherical-harmonic (S.H.) coefficients, as well as the conventional Legendre polynomials $P_n(\sin\phi)$ and the conventional associated Legendre functions $P_{nm}(\sin\phi)$, where ϕ denotes the geocentric latitude. With regard to the Legendre functions, the following transformations apply:

$$\overline{P}_n(\sin\phi) = (2n+1)^{\frac{1}{2}} P_n(\sin\phi) , \tag{A1.1a}$$

$$\overline{P}_{nm}(\sin\phi) = [2(2n+1)(n-m)!/(n+m)!]^{\frac{1}{2}} P_{nm}(\sin\phi) , \quad m \geq 1 . \tag{A1.1b}$$

The products between the S.H. coefficients and the corresponding Legendre functions are the same whether the conventional (unbarred) or the normalized (barred) quantities are utilized.

In using the formula

$$P_{nm}(\sin\phi) = \cos^m\phi \ P_n^{[m]}(\sin\phi) , \tag{A1.2}$$

where, for $m \leq n$,

$$p_n^{[m]}(\sin\phi) = d^m P_n(\sin\phi)/d(\sin\phi)^m \qquad (A1.3)$$

(for m>n this expression is zero), the following recurrent relationships have been utilized at AFGL, in which $P_n(\sin\phi)$, $P_n^{[m]}(\sin\phi)$ are written simply as P_n, $P_n^{[m]}$:

$$P_n = (1/n)[\sin\phi(2n-1)P_{n-1} - (n-1)P_{n-2}] , \qquad (A1.4)$$

$$P_n^{[m]} = P_{n-2}^{[m]} + (2n-1)P_{n-1}^{[m-1]} , \quad 2 \leq m \leq n-2 ; \qquad (A1.5)$$

for the special cases $m = 1$, $m = n - 1$, $m = n$ the formula (A1.5) becomes

$$P_n^{[1]} = P_{n-2}^{[1]} + (2n-1)P_{n-1} , \quad (m=1) \qquad (A1.6a)$$

$$P_n^{[n-1]} = (2n-1)P_{n-1}^{[n-2]} , \quad (m=n-1) \qquad (A1.6b)$$

$$P_n^{[n]} = (2n-1)P_{n-1}^{[n-1]} . \quad (m=n) \qquad (A1.6c)$$

The case $m = 0$ is treated in (A1.4) since $P_{n0} \equiv P_n^{[0]} \equiv P_n$ (see equations A1.2,3).

The two values needed to start the process (A1.4) are

$$P_0 = 1 , \quad P_1 = \sin\phi . \qquad (A1.7)$$

With regard to the subsequent computation of $P_n^{[m]}$, the case $m = 1$ is treated first according to (A1.6a). The starting values are

$$(P_0^{[1]} \equiv 0) , \quad P_1^{[1]} = 1 . \qquad (A1.8)$$

The first of these values is trivial (see equation A1.3) and is not stored; it is only used once in (A1.6a) for $n = 2$. Next, (A1.5) is utilized for each n (starting with $n = 2$) and for each m (starting with $m = 2$) except for the last two values of

-64-

m, in which case (A1.6b,c) are used instead. Thus for n = 2, only (A1.6c) is used in computing $P_2^{[2]}$; for n = 3, (A1.6b) gives $P_3^{[2]}$ and (A1.6c) gives $P_3^{[3]}$; but for any further functions, all of (A1.5) (A1.6b,c) are needed.

For large n and m, the values of P_{nm} and, especially, $P_n^{[m]}$ computed as above become exceedingly large. Already for n = 38 values emerge whose order of magnitude is 10^{70} and higher, leading to numerical difficulties because of the computer exponent limitations. The above formulas could safely be used to within a (36,36) expansion. Beyond that, the normalized functions should be used instead. New recurrent relations can be obtained from the previous formulas through a simple substitution for P_n , $P_n^{[m]}$ based on (A1.1a,b), namely

$$P_n = \overline{P}_n / (2n + 1)^{\frac{1}{2}} , \qquad (A1.9a)$$

$$P_{nm} = \{(n + m)! / [2(2n + 1)(n - m)!]\}^{\frac{1}{2}} \overline{P}_{nm} , \qquad m \geq 1 . \qquad (A1.9b)$$

Since, in analogy to (A1.2), it also holds true that

$$\overline{P}_{nm} = \cos^m \phi \ \overline{P}_n^{[m]} , \qquad (A1.10)$$

the formulas (A1.1b) and (A1.9b) relate $P_n^{[m]}$ and $\overline{P}_n^{[m]}$ as well. This will be understood throughout without any further statements to that effect.

Equation (A1.4) can now be rewritten with (A1.9a) taken into account, giving

$$\overline{P}_n = (2n + 1)^{\frac{1}{2}} (1/n) \{\sin\phi (2n - 1)^{\frac{1}{2}} \overline{P}_{n-1} - [(n - 1)/(2n - 3)^{\frac{1}{2}}] \overline{P}_{n-2}\} . \qquad (A1.11)$$

If (A1.5) - (A1.6c) are similarly rewritten with (A1.9a,b) taken into account, it follows that

$$\overline{P}_n^{[m]} = \{(2n + 1)/[(n + m - 1)(n + m)]\}^{\frac{1}{2}} \{[(n - m - 1)(n - m)/(2n - 3)]^{\frac{1}{2}} \overline{P}_{n-2}^{[m]}$$

$$+ (2n - 1)^{\frac{1}{2}} \overline{P}_{n-1}^{[m-1]}\} , \qquad 2 \leq m \leq n - 2 ; \qquad (A1.12)$$

-65-

$$\overline{P}_n^{[1]} = \{(2n+1)/[n(n+1)]\}^{\frac{1}{2}}\{[(n-2)(n-1)/(2n-3)]^{\frac{1}{2}}\overline{P}_{n-2}^{[1]} + [2(2n-1)]^{\frac{1}{2}}\overline{P}_{n-1}\} \, ,$$

$$(m = 1) \qquad\qquad (A1.13a)$$

$$\overline{P}_n^{[n-1]} = [(2n+1)/(2n-2)]^{\frac{1}{2}}\overline{P}_{n-1}^{[n-2]} \, , \qquad (m = n-1) \qquad\qquad (A1.13b)$$

$$\overline{P}_n^{[n]} = [(2n+1)/2n]^{\frac{1}{2}}\overline{P}_{n-1}^{[n-1]} \, . \qquad (m = n) \qquad\qquad (A1.13c)$$

Due to the presence of 2 in the factor of $\overline{P}_{n-1}$ in (A1.13a), this formula is not a special case of (A1.12), in the sense that it cannot be obtained upon replacing m in (A1.12) by 1 (this could have been done when passing from A1.5 to A1.6a).

In agreement with (A1.7) and (A1.1a), the starting values for (A1.11) are

$$\overline{P}_0 = 1 \, , \qquad \overline{P}_1 = \sqrt{3} \; \sin\phi \, . \qquad\qquad (A1.14)$$

Subsequently, in using (A1.1b) the values of $\overline{P}_n^{[m]}$ are computed in analogy to (A1.8) and the text that followed; the starting values are

$$(\overline{P}_0^{[1]} \equiv 0) \, , \qquad \overline{P}_1^{[1]} = \sqrt{3} \, . \qquad\qquad (A1.15)$$

Large numerical values are no longer a hindrance in proceeding in this fashion. However, for large n and m -- around 70 or 80 and higher -- the computational accuracy in $\overline{P}_n^{[m]}$ quickly deteriorates. This is due to the propagation of round-off errors since a great many values (on the order of 3,000 and higher) are generated from merely two starting values in (A1.15). Therefore, the present set of formulas could safely be used only to about a (70,70) expansion. Although this is a significant improvement compared to the previous situation, it does not fulfill the anticipated needs. Consequently, a new set of recurrent relations will be derived which can be used for any expansion in practice, certainly through the degree and order (180,180) and possibly much higher.

The basic idea behind the new approach is to use two starting values for each order (m) of the associated Legendre functions, similar to the recurrent strategy for Legendre polynomials. Thus in the case of the truncation $N = 180$, at most 178 values will be generated from two starting values. In particular, since one will proceed in the sequence $\bar{P}_m^{[m]}$, $\bar{P}_{m+1}^{[m]}$, ..., $\bar{P}_n^{[m]}$, the number of generated values varies from 178 for $m = 1$ ($\bar{P}_1^{[1]}$ and $\bar{P}_2^{[1]}$ are the starting values while $\bar{P}_3^{[1]}$, $\bar{P}_4^{[1]}$, ... , $\bar{P}_{180}^{[1]}$ are generated) to 1 for $m = 178$ ($\bar{P}_{178}^{[178]}$ and $\bar{P}_{179}^{[178]}$ are the starting values while only $\bar{P}_{180}^{[178]}$ is generated); no values are generated for $m = 179$ (both $\bar{P}_{179}^{[179]}$ and $\bar{P}_{180}^{[179]}$ are "starting" values) and for $m = 180$ ($\bar{P}_{180}^{[180]}$ is a "starting" value). Although there are essentially N-times as many starting values in this approach compared to that of the previous paragraphs, the great increase in accuracy is well worth the effort.

This development starts with the conventional Legendre functions. First, the relation (A.14) for Legendre polynomials is recapitulated as

$$nP_n = \sin\phi \ (2n - 1)P_{n-1} - (n - 1)P_{n-2} \ , \qquad n \geq 2 \ . \qquad (A1.16)$$

This formula can be found in standard textbooks such as [Spiegel, 1968] where it is essentially equation (25.20). The starting values are P_0 and P_1 as they appeared in (A1.7). Next, the basic relation for $P_n^{[m]}$ is presented as

$$(n - m)P_n^{[m]} = \sin\phi \ (2n - 1)P_{n-1}^{[m]} - (n + m - 1)P_{n-2}^{[m]} \ , \qquad n \geq m + 2 \ , \qquad (A1.17)$$

which is readily obtained from equation (26.12) in the same textbook. This formula is structured in complete analogy to (A1.16), which can be obtained from it merely by setting $m = 0$. The starting values, $P_m^{[m]}$ and $P_{m+1}^{[m]}$, can be evaluated with the aid of the standard formula appearing, e.g., as (1-62) in [Heiskanen and Moritz, 1967], which leads to

$$p_m^{[m]} = (1/2^m)(2m)!/m! = 1 \times 3 \ldots \times (2m-1) , \tag{A1.18a}$$

$$p_{m+1}^{[m]} = 1 \times 3 \ldots \times (2m+1)\sin\phi . \tag{A1.18b}$$

Here again, upon setting $m = 0$ one recovers the starting values (A1.7).

In utilizing (A1.9a) in (A1.16) it follows that

$$\overline{P}_n = (2n+1)^{\frac{1}{2}}(1/n)\{\sin\phi \, (2n-1)^{\frac{1}{2}}\overline{P}_{n-1} - [(n-1)/(2n-3)^{\frac{1}{2}}]\overline{P}_{n-2}\} , \tag{A1.19}$$

which is (A1.11) recapitulated here to show the parallel between the new recurrent relations for $\overline{P}_n$ and for $\overline{P}_n^{[m]}$ below. In considering (A1.1a), the overbarred starting values are

$$\overline{P}_0 = P_0 ,$$
$$\overline{P}_1 = \sqrt{3} \, P_1 ;$$

with P_0 and P_1 from (A1.7) this yields

$$\overline{P}_0 = 1 , \tag{A1.20a}$$

$$\overline{P}_1 = \sqrt{3} \sin\phi , \tag{A1.20b}$$

which were already seen in (A1.14). Equation (A1.19) with the starting values (A1.20a,b) is the final recurrent relation for the normalized Legendre polynomials.

In analogy to the above, upon utilizing (A1.9b) in (A1.17), after a few arithmetic operations one obtains

$$\overline{P}_n^{[m]} = \{(2n+1)/[(n+m)(n-m)]\}^{\frac{1}{2}}\{\sin\phi \, (2n-1)^{\frac{1}{2}}\overline{P}_{n-1}^{[m]} - [(n+m-1)(n-m-1)$$

$$/(2n-3)]^{\frac{1}{2}}\overline{P}_{n-2}^{[m]}\} , \qquad n \geq m+2 . \tag{A1.21}$$

-68-

It is again noticed that upon setting $m = 0$ equation (A1.19) is recovered. In considering (A1.1b), the overbarred starting values are

$$\overline{P}_m^{[m]} = [2(2m+1)/(2m)!]^{\frac{1}{2}} P_m^{[m]} , \qquad m \geq 1 ,$$

$$\overline{P}_{m+1}^{[m]} = [2(2m+3)/(2m+1)!]^{\frac{1}{2}} P_{m+1}^{[m]} , \qquad m \geq 1 ;$$

with $P_m^{[m]}$ and $P_{m+1}^{[m]}$ from (A1.18a,b) this yields

$$\overline{P}_m^{[m]} = [2(2m+1)]^{\frac{1}{2}}\{(1/2)(3/4)...[(2m-1)/2m]\}^{\frac{1}{2}} , \qquad m \geq 1 , \qquad (A1.22a)$$

$$\overline{P}_{m+1}^{[m]} = [2(2m+3)]^{\frac{1}{2}}\{(3/2)(5/4)...[(2m+1)/2m]\}^{\frac{1}{2}}\sin\phi , \qquad m \geq 1 . \qquad (A1.22b)$$

It is now apparent that (A1.20a,b) do not follow from (A1.22a,b) upon setting $m = 0$, due to the factor 2 within the first brackets of the latter. This is imputable to the factor 2 appearing in equations (A1.1b) and (A1.9b) which thus would not yield (A1.1a) and (A1.9a) if m were set to zero; this fact is then reflected in the equations that followed (A1.21) as compared to the equations that followed (A1.19). On the other hand, (A1.19) followed from (A1.21) for $m = 0$, just as (A1.16) followed from (A1.17) for such m, because when the transformation (A1.9b) was applied to (A1.17) in order to obtain (A1.21), the above factor 2 cancelled out.

Equation (A1.21) with the starting values (A1.22a,b) is the final recurrent relation for $\overline{P}_n^{[m]}$. The final recurrent relation for the normalized associated Legendre functions then follows immediately upon considering (A1.10). In particular, since no order other than m appears in (A1.21) this equation holds true equally well with $\overline{P}_{nm}$, $\overline{P}_{n-1,m}$ and $\overline{P}_{n-2,m}$ replacing $\overline{P}_n^{[m]}$, $\overline{P}_{n-1}^{[m]}$ and $\overline{P}_{n-2}^{[m]}$, respectively. Since the starting values are given by the relatively very simple formulas (A1.22a,b), where the number of factors within {} is m, their computation does not represent a heavy burden by any standards. In fact, without the

-69-

strategy of computing the starting values separately for each order, the
numerical evaluation of the normalized associated Legendre functions through
the degree and order considered in this analysis would have been impossible.

APPENDIX 2
CONSIDERATION OF SPECIAL "TIDAL POINT MASSES"
FOR MODELING OF TIDAL CONSTITUENTS

In [Blaha, 1984], Chapter 3, the tidal model used in the adjustment of satellite altimetry is given as

$$h_j = 0.9333\xi_j + 0.612 \times (\text{equilibrium tide})_j \, , \tag{A2.1}$$

where

h_j = surface tide for the constituent "j" ,

ξ_j = ocean tide for the constituent "j" .

The formula (A2.1), appearing in the above reference as (3.7a,b), can be used in conjunction with all the tidal constituents, long-period as well as diurnal and semidiurnal.

Since the computation of the equilibrium tide is simple and straightforward, one's attention is directed to the evaluation of the ocean tide in equation (A2.1). According to pages 48 and 49 in [Blaha, 1982], it follows that

$$\xi_j = A_j(\phi,\lambda)\cos[\alpha_j - \psi_j(\phi,\lambda)] \, ,$$

where

α_j = Greenwich argument,

$A_j(\phi,\lambda)$ = amplitude,

$\psi_j(\phi,\lambda)$ = Greenwich phase angle,

all pertaining to the constituent "j".

The above equation can be written as

$$\xi_j = \xi_{1_j} + \xi_{2_j} \, ,$$

(A2.2a)

with

$$\xi_{1_j} = \cos\alpha_j A_j(\phi,\lambda)\cos\psi_j(\phi,\lambda) \, ,$$

(A2.2b)

$$\xi_{2_j} = \sin\alpha_j A_j(\phi,\lambda)\sin\psi_j(\phi,\lambda) \, .$$

(A2.2c)

The functions F and G below can be expressed in terms of a spherical-harmonic series as was done in the above reference, namely

(A2.3a)

$$F(\phi,\lambda) \equiv A_j(\phi,\lambda)\cos\psi_j(\phi,\lambda) = \sum_{n=0}^{\infty} \sum_{m=0}^{n} (a_{j_{nm}} \cos m\lambda + b_{j_{nm}} \sin m\lambda)P_{nm}(\sin\phi) \, ,$$

(A2.3b)

$$G(\phi,\lambda) \equiv A_j(\phi,\lambda)\sin\psi_j(\phi,\lambda) = \sum_{n=0}^{\infty} \sum_{m=0}^{n} (c_{j_{nm}} \cos m\lambda + d_{j_{nm}} \sin m\lambda)P_{nm}(\sin\phi) \, ,$$

where $P_{nm}(\sin\phi)$ are the associated Legendre functions in the argument $\sin\phi$, ϕ and λ being the geocentric latitude and longitude, respectively.

If the functions F and G were given all over the globe, one could compute the spherical-harmonic (S.H.) tidal coefficients a, b, c, d (with appropriate indices) as follows:

$$\begin{Bmatrix} a_{j_{nm}} \\ b_{j_{nm}} \end{Bmatrix} = [(2n+1)/\underline{2\pi}][(n-m)!/(n+m)!]\iint_{o}[A_j(\tilde\phi,\tilde\lambda)\cos\psi_j(\tilde\phi,\tilde\lambda)]P_{nm}(\sin\tilde\phi)\begin{Bmatrix} \cos m\tilde\lambda \\ \sin m\tilde\lambda \end{Bmatrix}d\sigma \, ,$$

$$\begin{Bmatrix} c_{j_{nm}} \\ d_{j_{nm}} \end{Bmatrix} = [(2n+1)/\underline{2\pi}][(n-m)!/(n+m)!]\iint_{\sigma}[A_j(\tilde\phi,\tilde\lambda)\sin\psi_j(\tilde\phi,\tilde\lambda)]P_{nm}(\sin\tilde\phi)\begin{Bmatrix} \cos m\lambda \\ \sin m\lambda \end{Bmatrix}d\sigma \, ,$$

where the symbol $\underline{2\pi}$ implies 2π for m>0 and 4π for m=0; this double role would have been avoided by adopting the normalized S.H. coefficients and Legendre functions instead of the conventional ones as used above. The symbol " $\sim$ " indicates a point within $d\sigma$, σ representing the surface of the earth.

With the expansions (A2.3a,b), equations (A2.2a-c) yield

$$\xi_j = \cos\alpha_j \sum_{n=0}^{\infty} \sum_{m=0}^{n} (a_{j_{nm}} \cos m\lambda + b_{j_{nm}} \sin m\lambda) P_{nm}(\sin\phi)$$

$$+ \sin\alpha_j \sum_{n=0}^{\infty} \sum_{m=0}^{n} (c_{j_{nm}} \cos m\lambda + d_{j_{nm}} \sin m\lambda) P_{nm}(\sin\phi) .$$

(A2.4)

The parts following $\cos\alpha_j$ and $\sin\alpha_j$ in (A2.4) can be compared to the S.H. expansion of geoid undulations (N). However, it is assumed that a first-phase adjustment has been carried out so that the second-phase adjustment has as a "normal field" the gravity field given by the (n,n) S.H. expansion. With respect to such a field, the second-phase geoid undulations resolved through the degree n' are represented by

$$N' = R \sum_{k=n+1}^{n'} \sum_{m=0}^{k} (C_{km} \cos m\lambda + S_{km} \sin m\lambda) P_{km}(\sin\phi) ,$$

(A2.5)

where R is the earth's mean radius and ϕ, λ are the geocentric coordinates of the point of evaluation. The value of N' in (A2.5) thus corresponds to the bandwidth n+1 through n'. Since n is usually 14 or higher, the spherical approximation implied by (A2.5) is inconsequential.

The similarity between (A2.4) and (A2.5) is actually closer than what appears from the equations in their current form, especially from the form of (A2.4). The first-phase adjustment provides not only for the solution of the gravity field within the (n,n) S.H. expansion, but also for the solution of selected tidal

-73-

parameters to within some expansion of the S.H. tidal coefficients. The tidal parameters consist of the change in the relative amplitude and the change in the phase angle per tidal constituent; the degree and order of the underlying S.H. expansion of the tidal effects in the first phase is considered to be also (n,n), although this is not a requirement (the advantage of this choice stems from the Legendre functions having been already computed to within n,n degree and order due to the geoidal evaluations, and the same is true with respect to the multiple angle trigonometric functions). Accordingly, if one wished for the solution of the ocean tide within the bandwidth n+1 through n' as a follow-up to the first phase, the formula (A2.4) for a given tidal constituent (the explicit subscript j is dropped) would become:

$$\xi' = \cos\alpha \sum_{k=n+1}^{n'} \sum_{m=0}^{k} (a_{km}\cos m\lambda + b_{km}\sin m\lambda)P_{km}(\sin\phi)$$

$$+ \sin\alpha \sum_{k=n+1}^{n'} \sum_{m=0}^{k} (c_{km}\cos m\lambda + d_{km}\sin m\lambda)P_{km}(\sin\phi) \ . \tag{A2.6}$$

The complete analogy between the formula (A2.5) and either part of the formula (A2.6) is apparent.

The above analogy suggests that the second-phase treatment of tidal parameters could follow the lines similar to the second-phase treatment of gravity field parameters. The latter have been represented by point-mass (P.M.) magnitudes allowing the local effects to manifest themselves quite independently of other such effects some distance apart, due in part to the cut-off distance (spherical cap) beyond which the contribution of observations to a given P.M. parameter has been ignored by the algorithm. Accordingly, the tidal effects could also have a greater freedom to manifest themselves locally if parallel

-74-

formulas could be developed in terms of some "tidal point masses". The second-phase adjustment model in terms of the "regular" point masses reads

$$N_k' = (1/G) \sum_j (1/\ell_{kj})(kM)_j \ , \tag{A2.7}$$

where G is the average value of gravity on the earth's surface, "k" is the (observation) point where the geoid undulation is available, "j" is the location of the point mass whose magnitude is $(kM)_j$, and ℓ_{kj} is the (chord) distance between the points k and j. Since (A2.7) is used to approximate the model (A2.5), the analogy between (A2.5) and (A2.6) allows the latter to be similarly approximated by

$$\xi_k' = \cos\alpha \sum_j (1/\ell_{kj})t_{1_j} + \sin\alpha \sum_j (1/\ell_{kj})t_{2_j} \ . \tag{A2.8}$$

Here α remains the Greenwich argument and t_{1_j}, t_{2_j} represent the "tidal P.M. parameters", all pertaining to a given tidal constituent.

Since the geoid undulations and the effects of tidal constituents are mutually independent, so are the P.M. parameters and the tidal P.M. parameters for different constituents. The latter can thus be added into the system of normal equations following the former without affecting the bandwidth associated with a "regular" P.M. adjustment. However, the length of the band is greatly increased. If the tidal point masses should have the same locations as the "regular" point masses, the number of parameters would increase by 200% per constituent as is clear upon comparing the model equations (A2.7) and (A2.8). Where only the constituents M_2, N_2 and O_1 are considered, the increase would be 600%, so that the total number of parameters would be $7\times$("regular" number of P.M. parameters). Such an increase would be clearly prohibitive.

-75-

However, the tidal constituents have a much smaller effect on altimeter residuals than the geoid undulations (one to two orders of magnitude). Accordingly, a low density grid of tidal point masses would be sufficient for a simultaneous adjustment of geoidal and tidal effects. For example, one can consider a 2°-geoidal resolution corresponding approximately to a (90,90) S.H. expansion of the earth's gravity field contrasted to a 6°-tidal resolution corresponding approximately to a (30,30) S.H. expansion; the number of S.H. coefficients in the latter case is about nine-fold smaller than in the former case. The tidal resolution could have been lowered even further with respect to the geoidal resolution. Be that as it may, the number of tidal point masses is about 1/9 of the "regular" point masses; when multiplying this number by 6 (two parameters per constituent, three constituents), the increase in the number of parameters is about 67%, for a total of 1.67×("regular" number of parameters).

The dimensions in the P.M. algorithm have been recently increased to a maximum of 2000 P.M. parameters by virtue of the banded structure of normal equations. However, almost that many are needed for the P.M. adjustment in the Indian Ocean alone, i.e., about 1700 P.M. parameters including those that have to be used twice due to overlapping adjustment strips. Multiplying this number by 1.67 would result in a total number of parameters reaching about 2800. This number of parameters is still too great of a burden regarding the computer capacity.

Next consider a 8°-tidal resolution corresponding approximately to a (22,22) S.H. expansion. The tidal point masses would now be distributed in an 8"x8" equilateral grid and their number would be 1/16 of the "regular" P.M. parameters. The multiplication by 6 results in an increase of 37.5% in the number of parameters for a total of 1.375×("regular" number of parameters); in the above case of the Indian Ocean this implies some 2300 parameters. From the computer core standpoint an adjustment could become feasible. The algorithm would be similar

-76-

to the "regular" P.M. algorithm except for some self-evident modifications (see $\cos\alpha$ and $\sin\alpha$ in equation A2.8, the introduction of two parameters per location when treating a given constituent, etc.). The depth of the tidal point masses could again correspond to 0.8 of their horizontal separation (s); this would lead, similar to previous studies, to considering a spherical cap of the radius 1.5s when determining which observations should be ignored in conjunction with a given parameter, and would preserve the original bandwidth essentially unchanged.

However, from the practical point of view the above case would not have the desirable effect. The first-phase adjustment at AFGL is usually made in terms of a (14,14) S.H. expansion of the earth's potential, and a higher degree and order expansion, within perhaps a (20,20) model, is easily feasible. Due to the advantages already mentioned, the S.H. tidal expansion should be made to about the same degree and order. Thus, in view of a (20,20) S.H. expansion of tidal effects being essentially a part of the first-phase algorithm already, the above (22,22) expansion is of marginal usefulness. In other words, the computer core capacity would have to nearly double before tidal P.M. parameters in the second adjustment offered a tangible advantage.

APPENDIX 3
UTILIZATION OF SEASAT ALTIMETER RESIDUALS
IN DETECTING BATHYMETRIC ANOMALIES

As has been reported on numerous occasions, pronounced sea-bottom features are accompanied, at the sea-level surface, by localized roughness in the oceanic geoid. This fact is best illustrated by the presence of large negative altimeter residuals in the area where a satellite arc crosses an important trench, such as the Puerto Rico trench, the New Hebrides trench, the Aleutian trench and others. Such residuals were presented, for example, in the paper "SEASAT Altimeter Reductions for Detailed Determinations of the Oceanic Geoid" by G. Hadgigeorge, G. Blaha and T. P. Rooney at the 1980 AGU Fall Meeting.

A situation of this kind is schematically depicted in Fig. A, where the (14,14) geoid corresponds to a global spherical-harmonic (S.H.) adjustment of satellite altimetry. The (90,90) geoid, based on the residuals from the global adjustment, represents relatively small features, down to those whose half-wavelength is approximately 2°. This fairly detailed resolution can be achieved through the use of point masses (distributed in a $2^{\circ} \times 2^{\circ}$ equilateral grid), collocation predictions (in a $2^{\circ} \times 2^{\circ}$ equilateral grid) and other means. The two methods just mentioned are described in the AFGL report [Blaha, 1984]; the first method alone has also been the subject of several earlier AFGL reports and papers. Clearly, the above (14,14) and (90,90) S.H. expansions could be replaced by other suitable degree and order expansions describing the earth's gravity field to within the desired resolution.

The index "o" in Fig. A indicates "observed" quantities, which are the originally measured values improved through the orbital and tidal adjustment (but not the geoidal adjustment). The orbital adjustment is implied in the
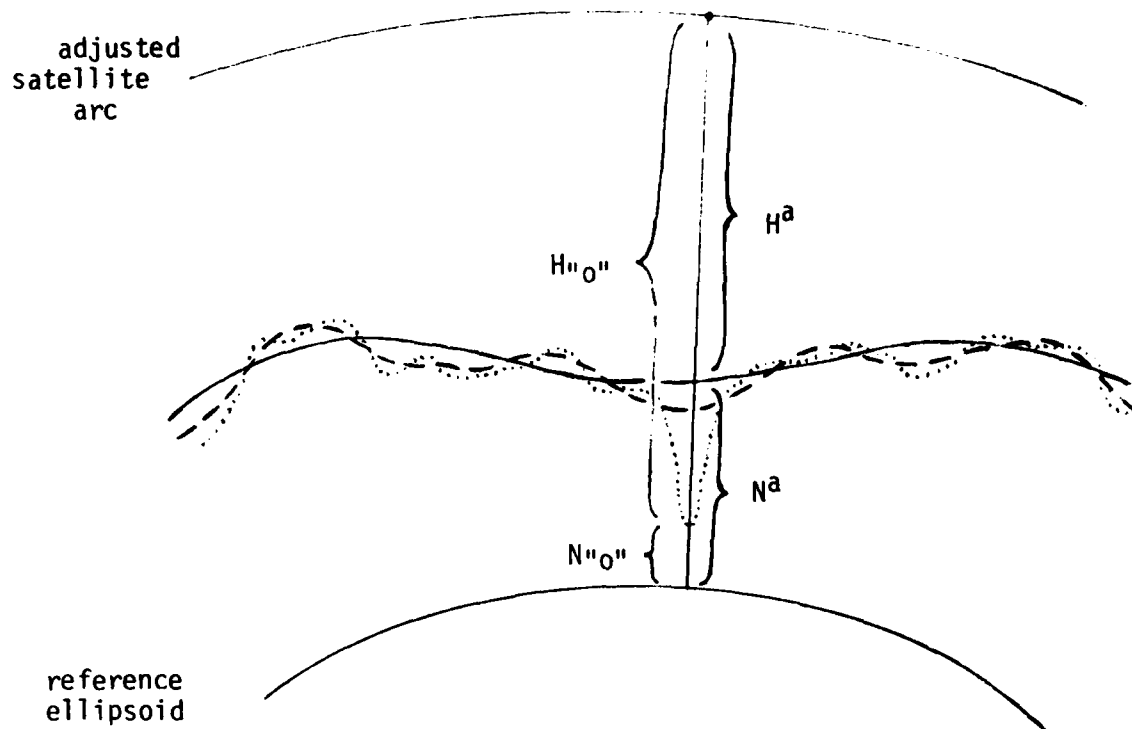
Fig. A

Schematic representation of satellite altimetry over a trench area

figure by the altimeter measurement associated with the adjusted -- as opposed to the initially given -- satellite arc. And the tidal adjustment is implied by considering the sea surface as free from tidal variations which are expressed by separate parameters. The superscript "a" indicates adjusted quantities, in particular, quantities linked to the (14,14) geoid as obtained in the global S.H. adjustment. Figure 2 of the AFGL report [Blaha, 1983] illustrates the "observed" and adjusted quantities in more detail. In the present context one need not be preoccupied with the improvement due to the tidal adjustment since it would amount, in open ocean, to merely a few decimeters. By comparison, the altimeter residuals over important trench areas are expected to be greater by one or two orders of magnitude.

Altimeter residuals will be denoted here by the symbol v_H. These quantities are treated as measurements in the subsequent determinations of the gravity field detail to be superimposed on the (14,14) S.H. representation, upon using the point-mass or collocation techniques as mentioned earlier. Denoting the geoidal residuals by the symbol v_N, one has

$$v_H = H^a - H_{"o"} \ , \tag{A3.1a}$$

$$v_N = N^a - N_{"o"} \ , \tag{A3.1b}$$

$$v_H = -v_N \ . \tag{A3.1c}$$

As depicted in Fig. A, a trench area induces large negative altimeter residuals,

$$v_N \ll 0 \ . \tag{A3.2}$$

These values are to be compared with the "one sigma" such as

$$\hat{\sigma} \simeq 3.2 \ m \ , \tag{A3.3}$$

which characterizes the geoidal detail neglected due to the (14,14) truncation of an infinite S.H. series. The description and estimation of this quantity can be found in Section 4.3 of [Blaha, 1984].

The three trench areas mentioned at the outset are 100-200 km wide and are associated with large negative altimeter residuals reaching typically between -10 m and -15 m in the vicinity of the trench axes. One could detect sea surface dips on this scale from a detailed geoidal map representing a 1°-resolution or better (1° corresponds to 111 km on the earth's surface). In order to detect dip areas 100 km wide, a $\frac{1}{2}^{\circ}$-resolution would be desirable. But such a procedure has a significant drawback imputable to the spatial distribution of SEASAT altimeter data. The ascending and descending passes form approximately a $1^{\circ} \times 1^{\circ}$ equilateral grid near the equator, providing for a strong 2°-resolution and a marginal 1°-resolution, but making any finer resolution impossible to achieve. In addition to its marginal geoidal representation, the 1°-resolution would still be too coarse for detecting relatively small but important ocean trench areas.

The notion of coarseness in this context is best illustrated by considering a 2°-resolution as obtained through a point-mass (P.M.) adjustment of the oceanic geoid. The observational density on SEASAT arcs is just under 2' in angular measure. Clearly, utilizing all of the altimeter data in the S.H. adjustment and, subsequently, in the P.M. adjustment would be computationally prohibitive. Furthermore, little would be gained from a configuration where the observational density along one dimension is over 30 times higher than the density along the other dimension. A practical conclusion has been reached to adopt every 16th point on each arc as selected input data in both adjustments. In this way, the separation between measurements along tracks becomes $\frac{1}{2}^{\circ}$, while the separation across tracks is fixed at 1°. This allows for a sufficient amount of spatial redundancy in the P.M. adjustment, especially in view of a 2°-resolution

-81-

(a 1°-resolution with the same data distribution would imply 50% redundancy along tracks and no redundancy across tracks).

The smoothing effect of a 2°-resolution could totally or partially obliterate the representation of a sea surface dip in the proximity of a trench. This has been noticed, for example, in the paper mentioned at the outset. The adjusted geoid in an extended Puerto Rico trench area covered with a $2^o \times 2^o$ equilateral grid of point masses did not exhibit any marked dip until it was saturated with additional point masses forming a localized $1^o \times 1^o$ equilateral grid. It is noteworthy that the geoidal dip associated with the Puerto Rico trench is pronounced (on the order of 15 m), that the trench area is relatively wide (approximately 200 km) and, especially, that the trench location is known beforehand. A less important trench might have gone unnoticed altogether.

The example of the Puerto Rico trench is overly optimistic, in that not only is the trench area wide and the location known, but also that the observational interval along tracks is $\frac{1}{4}^o$. This presents little computational burden by virtue of the regional extent of the adjustment, but the same cannot be said with regard to an adjustment of an entire ocean basin or the entire global ocean. One might hesitate to engage in the exercise of a global P.M. adjustment with quadruple the number of parameters (in view of the 1°-resolution) and double the number of data points (in view of $\frac{1}{4}^o$ data intervals along tracks) merely for the purpose of detecting several more, but by no means all, important trench areas.

However, even if one should choose to carry out such an exercise one would be well advised to consider the adjusted 1°-geoid together with the resulting (second-phase) residuals, especially if the detection of sea surface anomalies should not be limited to features whose width surpasses 100 km. But the adjusted P.M. geoid plus the corresponding residual equal the original altimeter residual from the global S.H. adjustment. This is apparent from Fig. A, where the

distance between the solid and the dotted curve is obtained by adding algebraical-
ly the two segments created by the dashed curve. Thus, the second-phase
techniques, such as the P.M. adjustment, collocation predictions, etc., can be
completely by-passed in the present task.

The use of the first-phase technique, i.e., the global S.H. altimeter ad-
justment, has a further significant advantage. In particular, a procedure has
been designed that takes into account every observation point (in approximately
2' intervals along tracks), not only points in $\frac{1}{2}^{\circ}$ or, perhaps, $\frac{1}{4}^{\circ}$ intervals.
Although the S.H. adjustment itself may utilize only data in $\frac{1}{2}^{\circ}$ intervals, the
remaining residuals can subsequently be filled in at every data location. These
high-density and high-resolution residuals can be examined for geoidal roughness
along the profiles, which has a crucial role to play in detecting bathymetric and
possibly other anomalies, such as geomagnetic anomalies.

The most promising in this respect is the detection of ocean trenches whose
presence is signalled by an abrupt dip in the sea surface. The importance of any
such dip is judged upon comparing the (first-phase) altimeter residuals with the
value $\hat{\sigma}$ linked to the truncation of the S.H. model. To be of any practical
advantage this value should be fairly low and, accordingly, the S.H. model should
be of a reasonably high degree and order. Equation (A3.3) indicates that the
(14,14) model is indeed satisfactory, considering that altimeter residuals at the
dip's location reach three to five times the magnitude of $\hat{\sigma}$.

The satellite arcs entering the S.H. adjustment are limited in length to
about 25° in angular measure or 7 minutes in duration as explained in Chapter 2
of [Blaha, 1981]. With the selected data points, a 25°-arc contains 54 obser-
vations in $\frac{1}{2}^{\circ}$-intervals, as opposed to over 850 original data points in 2'-inter-
vals. Since the (14,14) S.H. model corresponds approximately to a 13°-resolution,
the $\frac{1}{2}^{\circ}$ data interval could be replaced by a much larger interval without affecting

-83-

the S.H. adjustment itself. For example, one could use a 1°-interval and fill in the residuals at $\frac{1}{2}^{\circ}$- or shorter intervals as needed for subsequent determinations of a detailed gravity field. This would be done in the manner explained below in conjunction with the residuals filled in at all the original data points. A good resolution of the state vector parameters (six per arc) within this S.H. adjustment would then require a minimum arc length of 6° allowing for 7 or more altimeter observations.

On the other hand, the $\frac{1}{2}^{\circ}$-interval admits arcs as short as 3°, which is also the criterion of the minimum arc length from the standpoint of sufficient number of intersections with other arcs (see the above reference). This criterion allows for the utilization of 80-90% of all SEASAT arcs. During the actual S.H. adjustment of SEASAT altimetry at AFGL the observational interval has been chosen at $\frac{1}{2}^{\circ}$ and the minimum length criterion has been adopted as 3°. Accordingly, no filling in of residuals has been necessary for a subsequent P.M. adjustment or collocation predictions resulting in a 2°-geoid. The S.H. adjustment has encompassed some 6,700 arcs, of which about one-half have been 25° in length.

Since the S.H. adjustment can optionally solve for chosen tidal parameters as well, repeating tracks covering different phase angles of tidal constituents are particularly beneficial. However, in the detection of abrupt sea surface dips via the filled-in residuals the tidal effects are negligible and the repeating tracks lose much of their usefulness. Accordingly, a good percentage of arcs could be left out of consideration when examining these residuals. It is then quite natural to eliminate the shortest arcs whose state vectors are the most susceptible to contamination by the sea surface dip itself. By contrast, relatively long arcs crossing a trench area, such as $15^{\circ} - 25^{\circ}$ arcs, have only a small portion of their length exposed to the sea surface dip; this does not allow for any significant transfer of the negative anomaly from the residuals into the state vector parameters.

-84-

One can thus accomplish the double task -- eliminating both a number of unnecessary arcs and most of the arcs affected by sea surface dips themselves -- by adopting a minimum arc length of 15° (corresponding to about 500 original data points) for the purpose of this analysis. Even so, over two-thirds of all the SEASAT arcs will still be retained including those along repeating tracks. This criterion could, of course, be increased to 20° or another suitable length. Exceptionally, residuals on even a relatively long arc can be contaminated in the above sense if its ground track happens to coincide with the axis of an extended trench. But this is not cause for concern by virtue of the criss-crossing pattern of SEASAT tracks. If, for example, an ascending pass follows the direction of a trench, a descending pass will cross it, and will be able to detect the sea surface dip with maximum efficiency.

The simplest approach to filling in the residuals at data points not used in the global S.H. adjustment will now be described in detail. The crucial role in this task is played by the magnetic tape containing the original altimeter observations and the initial state vector (s.v.) parameters on each arc. According to previous statements, during the S.H. adjustment only one out of 16 observations on this tape constitutes the input quantity leading to the formulation of the pertinent observation equation and, eventually, to the final solution. In addition to the S.H. potential coefficients and selected tidal parameters, the solution also includes corrections to the s.v. parameters on each arc. The corrected s.v. parameters can then replace their initial values on this tape, or else should be recorded on a separate tape. The key role in the subsequent computation of the high-density residuals is played by the original observations coupled with the new s.v. parameters. These two kinds of quantities, optionally supplemented by the effect of tidal adjustment (deemed negligible in this context), lead directly to the values $H_{"o"}$ and $N_{"o"}$ depicted in Fig. A. The

adjusted S.H. coefficients (stored on another magnetic tape) give rise to the values H^a and N^a. Thus the values $v_H = -v_N$ from (A3.1a-c) can be computed at every original data point.

In practice this task can be accomplished with ease and efficiency upon undertaking what is essentially a new iteration in the S.H. adjustment process in which, however, only a few initial steps are carried out. The highlights of this process are:

a) all the altimeter observations are read and utilized;

b) the initial s.v. parameters are replaced by their adjusted values;

c) the initial S.H. coefficients are replaced by their adjusted values (a similar step could optionally take place with regard to the tidal parameters as well);

d) the adjustment routine proceeds to the formation of the constant terms of observation equations, stores them on a magnetic tape and stops;

e) these terms are the desired high-density altimeter residuals.

The last statement stems from the fact that the quantities called "constant terms" in conjunction with the initial values of parameters become residuals in conjunction with the final values of these parameters. As has transpired, the final values of the parameters have been obtained very economically by utilizing only one-sixteenth of the available data, but serve subsequently in the evaluation of the residuals corresponding to the entire data set. In spite of a great number of residuals to be evaluated, this step is exceedingly efficient when compared to the complete adjustment process.

Having now high-density and high-resolution altimeter residuals available, one is in a position to detect abrupt sea surface dips and evaluate their significance. This can lead to the detection of ocean trenches and other

anomalies. The altimeter residuals should be considered against the yardstick

of one sigma characterizing the geoidal resolution, such as $\hat{\sigma}$ presented in (A3.3).

Clearly, if the magnitude of the (negative) altimeter residuals is much larger

than $\hat{\sigma}$ over an extended area, e.g. over 100 km of a satellite profile, a presence

of a significant ocean trench is suspected.

In practical terms, the residuals can be scanned for large negative values

such as

$$v_H < -2\hat{\sigma} \ .$$

If several consecutive residuals along a given arc fit this characteristic, the

pertinent portion of the arc can be plotted with the rms residual also indicated.

The threshhold number of such consecutive residuals can be stipulated as 16,

corresponding to a $\frac{1}{2}^{\circ}$-segment of the profile. The above two scrutiny-type param-

eters, $-2\hat{\sigma}$ and $\frac{1}{2}^{\circ}$, are subject to change depending on the size of trenches one

wishes to detect. For the detection of deep and wide features of the sea surface

the magnitude of the two parameters can be increased. Conversely, for the detec-

tion of smaller features the magnitude would be lowered. However, since the

actual geoidal variations themselves (without the contribution of trenches) are

on the order of $\hat{\sigma}$ with respect to the adjusted (14,14) geoid, there is a limit

to the size of trenches and other anomalies one can detect with this method.

"Calibration" tests using known bathymetry, for example, could furnish quantita-

tive information with regard to this limitation.

REFERENCES

Blaha, G., SEASAT Altimetry Adjustment Model Including Tidal and Other Sea Surface Effects. AFGL Technical Report No. 81-0152, Air Force Geophysics Laboratory, Hanscom AFB, Massachusetts, 1981, ADA104188.

Blaha, G., Modeling and Adjusting Global Ocean Tides Using SEASAT Altimeter Data. AFGL Technical Report No. 82-0114, Air Force Geophysics Laboratory, Hanscom AFB, Massachusetts, 1982, ADA115841.

Blaha, G., Point-Mass Modeling of the Gravity Field with Emphasis on the Oceanic Geoid. AFGL Technical Report No. 83-0007, Air Force Geophysics Laboratory, Hanscom AFB, Massachusetts, 1983, ADA130535.

Blaha, G., First- and Second-Phase Gravity Field Solutions Based on Satellite Altimetry. AFGL Technical Report No. 84-0083, Air Force Geophysics Laboratory, Hanscom AFB, Massachusetts, 1984, ADA142256.

Estes, R. H., "A Simulation of Global Ocean Tide Recovery Using Altimeter Data with Systematic Orbit Error". Paper published in Marine Geodesy, Vol. 3, Nos. 1-4, Crane Russak, New York, 1980.

Heiskanen, W. A. and H. Moritz, Physical Geodesy. W. H. Freeman and Co., San Francisco, 1967.

Rapp, R. H., A Fortran Program for the Computation of Gravimetric Quantities from High Degree Spherical Harmonic Expansions. Report No. 334, Department of Geodetic Science and Surveying, The Ohio State University, Columbus, 1982.

Schwiderski, E. W., Global Ocean Tides, Part II: The Semidiurnal Principal Lunar Tide (M_2), Atlas of Tidal Charts and Maps. NSWC Technical Report No. 79-414, Naval Surface Weapons Center, Dahlgren, Virginia, 1979.

Spiegel, M. R., Mathematical Handbook of Formulas and Tables. Schaum's Outline Series, McGraw-Hill Book Co., New York, 1968.

Tscherning, C. C. and R. H. Rapp, Closed Covariance Expressions for Gravity Anomalies, Geoid Undulations, and Deflections of the Vertical Implied by Anomaly Degree Variance Models. Report No. 208, Department of Geodetic Science, The Ohio State University, Columbus, 1974.

END

FILMED

12-85

DTIC